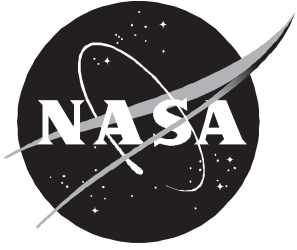


Stochastic Solution to Quantum Dynamics

Sarah John and John W. Wilson



Stochastic Solution to Quantum Dynamics

Sarah John
ViGYAN, Inc. • Hampton, Virginia

John W. Wilson
Langley Research Center • Hampton, Virginia

National Aeronautics and
Space Administration
Code JTT
Washington, D.C.
20546-0001

B U L K R A T E
POSTAGE & FEES PAID
NASA Permit No. G-27

Official Business
Penalty for Private Use, \$300

Postmaster: If undeliverable (Section 158 Postal Manual) Do Not Return

Abstract

The quantum Liouville equation in the Wigner representation is solved numerically by using Monte Carlo methods. For incremental time steps, the propagation is implemented as a classical evolution in phase space modified by a quantum correction. The correction, which is a momentum jump function, is simulated in the quasi-classical approximation via a stochastic process. In this paper the technique, which is developed and validated in two- and three-dimensional momentum space, extends an earlier one-dimensional work. Also, by developing a new algorithm, the application to bound state motion in an anharmonic quartic potential shows better agreement with exact solutions in two-dimensional phase space.

I. Introduction

Nuclear interaction theory is formulated in the language of quantum mechanics, and hence the development of general methods of solutions to quantum dynamics will provide useful tools for application to a large class of problems in nuclear many-body theory. Different approaches exist to the formulation of this complex problem, and attempts toward solutions at various levels of approximations are ongoing. The time-independent approach based on the Lippmann-Schwinger equation, for instance, is useful for describing systems with well-defined incident initial states (ref. 1). Similarly, the time-independent classical transport theory provides a method for calculating the fluence of particles as a superposition of sharply defined incident states under steady-state conditions (ref. 2). In real-life situations in deep-space radiations, for example, sporadic bursts of radiation may be encountered during which interactions and scattering proceed as fast transient events. This is in contrast with the slow variation of background space radiation for which a time-independent approach to study the effects of radiation on spacecraft is indicated. With this report we begin the development of a practical numerical code that is designed for the study of time-dependent nuclear scattering and interaction for transient thermodynamic wide spectrum radiation that is aimed toward application to the NASA radiation protection program for space travelers.

The density operator formalism of quantum dynamics (ref. 3) provides a suitable framework for the study of thermodynamic systems. In the Wigner representation (refs. 4–7), the dynamic equation of the density operator, given by the quantum Liouville equation, is transformed into ordinary functions and operators in phase-space coordinates. In a series expansion in powers of Planck's constant \hbar , the equation then provides an intuitively appealing reduction to the classical Liouville equation in the classical limit. Also, the more familiar equations appearing in nuclear scattering and heavy-ion collision theory, such as the hydrodynamic equations (see refs. 5 and 8) and the Boltzmann-Vlasov equations, may be extracted from the Wigner formalism. Because many of the cross sections used in the space program are derived from Monte Carlo simulation of the classical Boltzmann transport theory (ref. 9), the quantum correction to classical theory is of interest to NASA.

In this paper Monte Carlo methods are applied to solve the quantum Liouville equation in the Wigner representation (refs. 10 and 11). The equations are in a noncovariant form and apply to single-particle dynamics only. The time evolution is treated as a stochastic process, as seen in references 7 and 10–12. In an effort to simplify the problem, only first-order quantum effects are considered; and in this approximation the solution is applicable to quasi-classical systems (refs. 11, 13, and 14) that exhibit smoothly varying momentum distribution typical of highly mixed thermodynamic systems. In general, however, the first-order quantum correction may

not be sufficient and may, in some instances, even require the entire series summation (refs. 15 and 16). For the scattering of a highly collimated beam, for example, higher order terms become increasingly significant. Therefore, the method pursued in this work will hopefully complement the other approaches mentioned earlier.

A generalized Monte Carlo method was introduced in references 10 and 11. This paper extends that work to two and three dimensions, and a new algorithm is developed that gives improved results for the application considered.

In section II, quantum dynamics in the Wigner representation is reviewed and the stochastic techniques are developed. In section III, the technique is validated independently of the classical motion by comparing it with analytic solutions in the one-, two-, and three-dimensional momentum space. In section IV, an application to bound state motion within an anharmonic quartic potential in two-dimensional phase space is considered and the algorithm is discussed. In section V, the results and a discussion are presented, and in section VI, some concluding remarks and future applications are briefly indicated.

II. Theory

Quantum Liouville Equation (QLE)

The density operator $\hat{\rho}$ of a quantum thermodynamical system is given by

$$\hat{\rho} = \sum_m P_m |\psi_m\rangle\langle\psi_m| \quad (1)$$

where P_m is the probability for an ensemble element to be in eigenstate $|\psi_m\rangle$. The time evolution of $\hat{\rho}$ is the quantum Liouville equation,

$$i \frac{\partial \hat{\rho}}{\partial t} = [\hat{H}, \hat{\rho}] \quad (2)$$

where t denotes time, \hat{H} is the Hamiltonian, and $\hbar = 1$. Equation (2) has the formal solution

$$\hat{\rho}(t) = e^{-i\hat{H}t} \hat{\rho}(0) e^{i\hat{H}t} \quad (3)$$

Because the components of \hat{H} are usually noncommutative, this form is difficult to solve in practice. An intuitively appealing solution can be obtained by taking the Wigner transform of the QLE, which provides a series expansion in \hbar and reduces to the classical Liouville equation in the classical limit, $\hbar \rightarrow 0$.

Wigner Representation of QLE

A few basic properties of the Wigner transform are now reviewed. The Wigner transform of an operator, \hat{O} is defined by

$$O_w(\mathbf{x}, \mathbf{p}, t) = \int_{-\infty}^{\infty} d\mathbf{y} e^{i\mathbf{p}\cdot\mathbf{y}} \langle \mathbf{x} - \frac{1}{2}\mathbf{y} | \hat{O}(t) | \mathbf{x} + \frac{1}{2}\mathbf{y} \rangle \quad (4)$$

which is a simultaneous representation in both position coordinates \mathbf{x} and momentum coordinates \mathbf{p} . The Wigner transform for the density operator $\hat{\rho}$ is

$$f_w(\mathbf{x}, \mathbf{p}, t) = \int_{-\infty}^{\infty} d\mathbf{y} e^{i\mathbf{p}\cdot\mathbf{y}} \langle \mathbf{x} - \frac{1}{2}\mathbf{y} | \hat{\rho}(t) | \mathbf{x} + \frac{1}{2}\mathbf{y} \rangle \quad (5)$$

and is called the Wigner distribution function (generally defined with a normalization factor $(2\pi)^{-3}$). As an example, the Wigner transform of the density operator corresponding to a minimum wave packet defined by

$$\psi(\mathbf{x}) = \frac{1}{(2\pi\sigma^2)^{3/2}} \exp \left[-i\mathbf{p}_0 \cdot \mathbf{x} - \frac{(\mathbf{x} - \mathbf{x}_0)^2}{4\sigma^2} \right] \quad (6)$$

is given by

$$\begin{aligned} f_w(\mathbf{x}, \mathbf{p}, t) &= \int_{-\infty}^{\infty} d\mathbf{y} e^{i\mathbf{p} \cdot \mathbf{y}} \psi^* \left(\mathbf{x} - \frac{1}{2}\mathbf{y} \right) \psi \left(\mathbf{x} + \frac{1}{2}\mathbf{y} \right) \\ &= 2 \exp \left[-2\sigma^2 (\mathbf{p} - \mathbf{p}_0)^2 - \frac{(\mathbf{x} - \mathbf{x}_0)^2}{2\sigma^2} \right] \end{aligned} \quad (7)$$

The Wigner function has many analogs with the classical distribution function. For example,

$$(2\pi)^{-3} \int d\mathbf{p} f_w(\mathbf{x}, \mathbf{p}, t) = \langle \mathbf{x} | \hat{\rho} | \mathbf{x} \rangle \quad (8)$$

$$(2\pi)^{-3} \int d\mathbf{x} f_w(\mathbf{x}, \mathbf{p}, t) = \langle \mathbf{p} | \hat{\rho} | \mathbf{p} \rangle \quad (9)$$

$$(2\pi)^{-3} \int d\mathbf{x} d\mathbf{p} f_w(\mathbf{x}, \mathbf{p}, t) = 1 \quad (10)$$

and the expectation value of an observable \hat{O} is given by

$$\langle \hat{O}(t) \rangle = (2\pi)^{-3} \int d\mathbf{x} d\mathbf{p} O_w(\mathbf{x}, \mathbf{p}, t) f_w(\mathbf{x}, \mathbf{p}, t) \quad (11)$$

However, even though $f_w(\mathbf{x}, \mathbf{p}, t)$ is real (that is, $f_w^* = f_w$) it cannot strictly be a distribution function because it can have negative values, and therefore the Wigner function should at most be considered as an auxiliary function that is useful for calculating thermodynamic averages.

The Wigner transform of the quantum Liouville equation becomes

$$\frac{\partial f_w}{\partial t}(\mathbf{x}, \mathbf{p}, t) = -2H_w \sin \left(\frac{\Lambda}{2} \right) f_w(\mathbf{x}, \mathbf{p}, t) \quad (12)$$

in which H_w is the Wigner transformed Hamiltonian and Λ is the Poisson bracket operator given as

$$\Lambda = \overleftarrow{\nabla}_{\mathbf{p}} \cdot \overrightarrow{\nabla}_{\mathbf{x}} - \overleftarrow{\nabla}_{\mathbf{x}} \cdot \overrightarrow{\nabla}_{\mathbf{p}} \quad (13)$$

where the arrows indicate the direction of action of the operator. Expanding the sine term gives the series expansion

$$\frac{\partial f_w}{\partial t}(\mathbf{x}, \mathbf{p}, t) = \left(-H_w \Lambda + \frac{1}{24} H_w \Lambda^3 - \frac{1}{1920} H_w \Lambda^5 + \dots \right) f_w(\mathbf{x}, \mathbf{p}, t) - (\mathcal{L}_c + \mathcal{L}_q) f_w(\mathbf{x}, \mathbf{p}, t) \quad (14)$$

where $\mathcal{L}_c = H_w \Lambda$ is the classical Liouville operator and $-\mathcal{L}_q$ (which is equal to all higher order terms) is the quantum operator. The solution to equation (14) is given by

$$f_w(\mathbf{x}, \mathbf{p}, t) = e^{-(\mathcal{L}_c + \mathcal{L}_q)t} f_w(\mathbf{x}, \mathbf{p}, 0) \quad (15)$$

For small increments of time, equation (15) becomes

$$f_w(\mathbf{x}, \mathbf{p}, \Delta t) = e^{-\mathcal{L}_q \Delta t} e^{-\mathcal{L}_c \Delta t} f_w(\mathbf{x}, \mathbf{p}, 0) + \mathcal{O}(\Delta t^2) \quad (16)$$

Hence, infinitesimal time motion can be described in terms of successive classical and quantum evolutions in which the classical operator transforms the function to

$$f_{wc}(\mathbf{x}, \mathbf{p}, \Delta t) = e^{-\mathcal{L}_c \Delta t} f_w(\mathbf{x}, \mathbf{p}, 0) \quad (17)$$

and the quantum operator acts on f_{wc} , thus giving

$$f_w(\mathbf{x}, \mathbf{p}, \Delta t) = e^{-\mathcal{L}_q \Delta t} f_{wc}(\mathbf{x}, \mathbf{p}, \Delta t) \quad (18)$$

These expressions are difficult to evaluate analytically for arbitrary functions. Hence, Monte Carlo methods are applied with the advantage that the only analytic evaluation required is that for the action of the operators on a delta function. Explicit expressions for the operators \mathcal{L}_c and \mathcal{L}_q for a Hamiltonian operator of the form

$$\hat{H} = \frac{\hat{\mathbf{p}}^2}{2m} + V(\hat{\mathbf{x}}) \quad (19)$$

with Wigner transform

$$H_w(\mathbf{x}, \mathbf{p}) = \frac{\mathbf{p}^2}{2m} + V(\mathbf{x}) \quad (20)$$

(where \mathbf{x} and \mathbf{p} are now variables and not operators) are obtained as

$$\mathcal{L}_c = \frac{\mathbf{p}}{m} \cdot \vec{\nabla}_{\mathbf{x}} - \left(\vec{\nabla}_{\mathbf{x}} V \right) \cdot \vec{\nabla}_{\mathbf{p}} \quad (21)$$

$$\mathcal{L}_q = \frac{1}{24} V(\mathbf{x}) \left(\vec{\nabla}_{\mathbf{x}} \cdot \vec{\nabla}_{\mathbf{p}} \right)^3 + \dots \quad (22)$$

The action of \mathcal{L}_c on the delta function is standard. The action of \mathcal{L}_q on the delta function is now evaluated explicitly in the quasi-classical limit for a central potential $V(r)$ with $r = |\mathbf{x} - \mathbf{x}_i|$ and,

$$\mathcal{L}_q = \frac{1}{24} V(r) \left(\vec{\nabla}_{\mathbf{x}} \cdot \vec{\nabla}_{\mathbf{p}} \right)^3 \quad (23)$$

Expanding \mathcal{L}_q in terms of the radial component p_0 and the perpendicular components p_1 and p_2 of the momentum (appendix A) gives

$$\mathcal{L}_q = \mathcal{L}_{q1} + \mathcal{L}_{q2} \quad (24)$$

where

$$\mathcal{L}_{q1} = \frac{a_L}{2} \partial_{p_0}^3 + a_T \partial_{p_0} \partial_{p_1}^2 \quad (25)$$

$$\mathcal{L}_{q2} = \frac{a_L}{2} \partial_{p_0}^3 + a_T \partial_{p_0} \partial_{p_2}^2 \quad (26)$$

with

$$a_L = \frac{1}{24} \frac{\partial^3 V}{\partial r^3} \quad (27)$$

$$a_T = \frac{1}{8} \frac{\partial}{\partial r} \left(\frac{1}{r} \frac{\partial V}{\partial r} \right) \quad (28)$$

Consider first the action of \mathcal{L}_{q_1} on the delta function. (Similar arguments hold for \mathcal{L}_{q_2} .) It acts on the p_0 and p_1 components only, thus giving

$$\begin{aligned} \mathcal{J}(\mathbf{p} - \mathbf{p}_i) &\equiv e^{-\mathcal{L}_{q_1} t} \delta(\mathbf{p} - \mathbf{p}_i) \\ &= \delta(p_2 - p_{2i}) e^{-\mathcal{L}_{q_1} t} \delta(p_0 - p_{0i}) \delta(p_1 - p_{1i}) \end{aligned} \quad (29)$$

A change of variables to $v_0 = p_0 + \gamma p_1$ and $v_1 = p_0 - \gamma p_1$ reduces the expression to a product of one-dimensional forms. The operator \mathcal{L}_{q_1} transforms into

$$\mathcal{L}_{q_1} = a \partial_{v_0}^3 + a \partial_{v_1}^3 \quad (30)$$

where

$$a = \frac{a_L}{2} + a_T \gamma^2 = 2a_L \quad (31)$$

with

$$\gamma = \left(\frac{3a_L}{2a_T} \right)^{1/2} \quad (32)$$

and equation (29) transforms into

$$\mathcal{J}(\mathbf{p} - \mathbf{p}_i) \rightarrow 2\gamma \delta(p_2 - p_{2i}) e^{-at \partial_{v_0}^3} \delta(v_0 - v_{0i}) e^{-at \partial_{v_1}^3} \delta(v_1 - v_{1i}) \quad (33)$$

where 2γ is the Jacobian of the transformation for the delta functions.

The expressions to be evaluated are of the typical one-dimensional form with at replaced by a . Thus,

$$\begin{aligned} Ai(a; p - p_i) &= e^{-a \partial_p^3} \delta(p - p_i) \\ &= \frac{1}{2\pi} \int_{-\infty}^{\infty} dy e^{iay^3 + ipy} \end{aligned} \quad (34)$$

where Ai is recognized as the Airy function. Depending on the sign of a , the function decreases exponentially along one direction and is oscillatory along the other with a slow decay in amplitude and increasing frequency.

Monte Carlo Method

In a Monte Carlo procedure a sample set of test points is selected to represent the initial positive valued function. Thus,

$$f_w(\mathbf{x}, \mathbf{p}, 0) \approx \frac{(2\pi)^3}{N} \sum_{i=1}^N \sigma_i \delta(\mathbf{x} - \mathbf{x}_i) \delta(\mathbf{p} - \mathbf{p}_i) \quad (35)$$

where $\sigma_i = 1$ is the sign of the test point because, as noted above, $f_w(\mathbf{x}, \mathbf{p}, t)$ may be positive or negative. The classical propagation is a canonical contact transformation that transports the delta functions to new positions along deterministic trajectories so that

$$f_{wc}(\mathbf{x}, \mathbf{p}, \Delta t) = \frac{(2\pi)^3}{N} \sum_i \sigma_i \delta(\mathbf{x} - \mathbf{x}_{ci}) \delta(\mathbf{p} - \mathbf{p}_{ci}) \quad (36)$$

where \mathbf{x}_{ci} and \mathbf{p}_{ci} are evaluated via Hamilton's equations of motion

$$\left. \begin{aligned} \frac{d\mathbf{x}_i}{dt} &= \frac{\partial H}{\partial \mathbf{p}_i} \\ \frac{d\mathbf{p}_i}{dt} &= -\frac{\partial H}{\partial \mathbf{x}_i} \end{aligned} \right\} \quad (37)$$

To implement the quantum correction as given by equation (34), a strong damping for the Airy functions is useful. (Details for only the one-dimensional quantum jump function are discussed here. For higher dimensions see section III.) Now the phase space assumes a graininess due to the delta function representation; that is, the larger the number of representative points, the finer the grain structure. For a coarse-grained analysis of the quantum correction, note that the increasing rapidity of the oscillation of the Airy function at large momentum distances implies a net cancellation. Hence, to speed simulation, a grain size is introduced into the $\delta(p - p_i)$ term to produce a faster damping rate for the function. This is achieved by approximating the delta function by a narrow-width Gaussian function, which modifies the Airy function to

$$\mathcal{J}_\alpha(a; p - p_i) = e^{-at\delta_p^3} \delta_\alpha(p - p_i) \quad (38)$$

where $\delta_\alpha(p - p_i)$ is the Gaussian function of width α . The expressions for the modified Airy functions \mathcal{J}_α are given in appendix B.

The corresponding quantum jump function is defined as

$$J_\alpha(a; p - p_i) = \mathcal{J}_\alpha(a; p - p_i) - \delta_\alpha(p - p_i) \quad (39)$$

Figure 1(a) illustrates a typical Gaussian-modified Airy function, and figure 1(b) illustrates the corresponding quantum jump function $J_\alpha(a; p)$, which is shown as “ J ” in the figures.

The jump function is implemented via a stochastic simulation. To this end, let J_\pm correspond to the positive and negative segments of the function J_α . Partial integration easily shows that,

$$\int J_\alpha(a; p - p_i) dp = 0 \quad (40)$$

which indicates that the areas under the positive and negative segments are equal. Defining the area A gives

$$A = \int |J_\pm| dp \quad (41)$$

and rewriting equation (39) by using equations (40) and (41) gives

$$\begin{aligned} J_\alpha(a; p - p_i) &= A \left[\frac{|J_+|}{A} - \frac{|J_-|}{A} \right] \\ &= A[F_+ - F_-] \end{aligned} \quad (42)$$

which defines the jump “probability” functions as $F_\pm(a; p - p_i) = |J_\pm|/A$.

The stochastic method is based on the following probabilistic interpretation. For the two random variables X and Y , the joint probability $P(X, Y)$ is given by

$$P(X, Y) = P(X|Y)P(Y) \quad (43)$$

where $P(Y)$ is the probability for the event Y and $P(X|Y)$ is the conditional probability for the event X , provided that event Y has occurred. Compare equation (43) with equation (42). If $A < 1$, interpret $P(Y) = A$ as the probability for the quantum event, or as the creation probability. In other words, only the test points selected randomly with probability $P(Y)$ undergo quantum events during each time interval. (That is, if $A > 1$, let $A = n + \mathcal{A}$, where n is an integer, and $\mathcal{A} < 1$. Then, the test point will undergo quantum events n times and $P(Y) = \mathcal{A}$ will determine whether an additional quantum event should take place.) Generally, a is small enough (see fig. 2) to ensure that $A < 1$ so that, at most, one quantum event occurs per time step.

The conditional probability $P(X|Y) = F_+ - F_-$ represents the momentum jump probability corresponding to the random variable $X \equiv p$. A pair of values Δp_{\pm} is selected randomly by using the cumulative distributions for F_{\pm} . In the Monte Carlo representation, this becomes a test pair with coordinates,

$$\delta(p - (p_{ci} + \Delta p_{\pm})) \delta(x - x_{ci}) \sigma_i \sigma_{\pm}$$

where $\sigma_{\pm} = \pm 1$ for the positive and negative points. The newly created points are appended to the initial set to undergo subsequent classical and quantum motions. If $A \ll 1$, a factor M is introduced to enhance the creation probability to MA , with a normalization factor $1/M$ for the new pairs.

Clearly, in the absence of the classical motion, the stochastic process is a Markoff process. That is, with $t_{n-1} < t_n$,

$$F \{p(t_n) \leq p_n | p(t), t \leq t_{n-1}\} = F \{p(t_n) \leq p_n | p(t_{n-1})\}$$

The jump probability for each test point is thus independent of its past history, and depends only on its present location in momentum space.

III. Validation of Stochastic Quantum Motion

The validity of the technique developed in the previous section is established by comparing stochastic quantum time development in momentum space with analytic solutions. This is easily done when the initial function is a Gaussian.

One-Dimensional Quantum Motion

The quantum time development for the interval t in the quasi-classical approximation is given by

$$f(p, t) = e^{-at\partial_p^3} f(p, 0) \quad (44)$$

With the initial function given by

$$f(p, 0) = \frac{1}{\sqrt{2\pi\alpha}} e^{-p^2/2\alpha^2} \quad (45)$$

the analytic solution is the Gaussian modified Airy function given in appendix B.

For the stochastic evolution, a representative set of points for the initial function is chosen as follows: A pair of values (p_i, f_i) is selected randomly within a specified boundary for f and p such that f lies well within the defined area. The function f varies from 0 to $f_{\max} = 1/(\sqrt{2\pi\alpha})$. If $f(p_i) < f_i$, then p_i is selected; otherwise, it is discarded. Hence,

$$f(p, 0) \approx \frac{2\pi}{N} \sum_{i=1}^N \delta_{\alpha'}(p - p_i) \quad (46)$$

where the test Gaussian functions have width α' with $\alpha' \ll \alpha$. By dividing the total time t into K discrete time intervals ($\Delta t = t/K$), the time development is written as

$$f(p, t) = \left(e^{-a \Delta t \partial_p^3} \right)^K f(p, 0) \quad (47)$$

During each time step, statistical test points are selected with probability A (see the discussion following eq. (42)) and the new test pairs are created at $p_i + \Delta p_{\pm}$, where values of Δp_{\pm} are selected with conditional probability F_{\pm} which get appended to the main list. The updated list is propagated in the subsequent time interval.

In the actual algorithm, the momentum space is divided into grids and the test points are assigned on it. With $at = 0.1$ and $a \Delta t = 0.001$, 100 time steps are executed. The creation probability is enhanced by an arbitrary factor M that is set at $M = 10000/N$. Thus, for 100 initial test points the creation probability is increased 100 times; that is, the smaller the number of initial points, the larger the number of pair creations. Each representative pair for $J_{\alpha}(a \Delta t; p - p_i)$ is therefore given by

$$\frac{1}{M} [\delta(p - (p_i + \Delta p_{+})) - \delta(p - (p_i + \Delta p_{-}))]$$

For a density k on the grids, the process is repeated k times.

Figure 3 compares the results with the analytic solutions for various grid sizes, the initial number of test points N , and for various Gaussian widths α' for the test points. The results show good agreement with the analytic solutions and appear to be independent of the variables.

Two-Dimensional Quantum Motion

The two-dimensional quantum motion is given by

$$f(p_0, p_1, t) = e^{-\mathcal{L}_q t} f(p_0, p_1, 0) \quad (48)$$

where p_0 and p_1 are the radial and perpendicular components, respectively, and \mathcal{L}_q is given by equation (25) with $a_L/2$ replaced by a_L . The initial function is chosen to be

$$f(p_0, p_1, 0) = \frac{1}{2\pi\alpha^2} \exp \left[\frac{-(p_0^2 + p_1^2)}{2\alpha^2} \right] \quad (49)$$

To obtain the analytic solution, change the variables to $v_0 = p_0 + p_1$, and $v_1 = p_0 - p_1$. Thus,

$$\tilde{f}(v_0, v_1, t) = \frac{1}{2\pi\alpha^2} \left(e^{-at\partial_{v_0}^3} e^{-\frac{v_0^2}{4\alpha^2}} \right) \left(e^{-at\partial_{v_1}^3} e^{-\frac{v_1^2}{4\alpha^2}} \right) \quad (50)$$

which is recognized as a product of one-dimensional forms. The inverse transformation is then computed to get the analytic solution. (See fig. 4.)

For the stochastic evolution, consider the action of \mathcal{L}_q on a test point during the subinterval Δt given by

$$\mathcal{J}_{\alpha}(a \Delta t; \mathbf{p} - \mathbf{p}_i) = e^{-\mathcal{L}_q \Delta t} \delta(p_0 - p_{0i}) \delta(p_1 - p_{1i}) \quad (51)$$

Transforming to variables v_0 and v_1 as before gives

$$\begin{aligned} \mathcal{J}_\alpha(a \Delta t; \mathbf{p} - \mathbf{p}_i) &\rightarrow 2 \left[e^{-a \Delta t \partial_{v_0}^3} \delta_{\alpha'}(v_0 - v_{0i}) \right] \left[e^{-a \Delta t \partial_{v_1}^3} \delta_{\alpha'}(v_1 - v_{1i}) \right] \\ &= 2 [J_{\alpha'}(v_0 - v_{0i}) + \delta_{\alpha'}(v_0 - v_{0i})] [J_{\alpha'}(v_1 - v_{1i}) + \delta_{\alpha'}(v_1 - v_{1i})] \end{aligned} \quad (52)$$

which to $\mathcal{O}(\Delta t)$ gives

$$\mathcal{J}_\alpha(a \Delta t; \mathbf{p} - \mathbf{p}_i) = 2 [J_{\alpha'}(v_0 - v_{0i}) \delta_{\alpha'}(v_1 - v_{1i}) + J_{\alpha'}(v_1 - v_{1i}) \delta_{\alpha'}(v_0 - v_{0i}) + \delta_{\alpha'}(v_0 - v_{0i}) \delta_{\alpha'}(v_1 - v_{1i})] \quad (53)$$

because $J_{\alpha'}$ is of $\mathcal{O}(\Delta t)$. The pair selection for each $J_{\alpha'}$ is done as before and the representative test pairs are

$$\delta(v_1 - v_{1i}) \delta(v_0 - (v_{0i} + \Delta v_{0\pm})) \sigma_{\pm} \sigma_i + \delta(v_0 - v_{0i}) \delta(v_1 - (v_{1i} + \Delta v_{1\pm})) \sigma_{\pm} \sigma_i$$

Note that two pairs are created for each event expressed by the two summations. Transforming back to the original coordinates gives the representative test pairs

$$\delta\left(p_0 - \left(p_{0i} + \frac{\Delta v_{0\pm}}{2}\right)\right) \delta\left(p_1 - \left(p_{1i} + \frac{\Delta v_{0\pm}}{2}\right)\right) \sigma_{\pm} \sigma_i + \delta\left(p_0 - \left(p_{0i} + \frac{\Delta v_{1\pm}}{2}\right)\right) \delta\left(p_1 - \left(p_{1i} - \frac{\Delta v_{1\pm}}{2}\right)\right) \sigma_{\pm} \sigma_i$$

Figures 5(a) and 5(b), which show the results for stochastic simulation, compare well with figures 4(a) and 4(b), respectively. As before, 100 time steps were executed, and the pair creation probability was enhanced by a factor of 20 by using an initial number of 10 000 test points. The effect of increasing the width parameter α' on the simulation is seen by comparing figures 5(a) and 5(b) with figures 5(c) and 5(d). The effect of increasing grid size is seen in comparing figures 5(a) and 5(b) with figures 5(e) and 5(f). Although a 25-percent increase in width α' has little effect on the solution, the use of a 33-percent larger grid lowers the distribution peaks, as can be seen when comparing figure 5(f) with figure 5(b).

Three-Dimensional Quantum Motion

The three-dimensional quantum motion is given by

$$f(\mathbf{p}, t) = e^{-\mathcal{L}_q t} f(\mathbf{p}, 0) \quad (54)$$

The initial Gaussian function may be written in terms of parallel and perpendicular components. Thus,

$$f(\mathbf{p}, 0) = \frac{1}{(\sqrt{2\pi}\alpha)^3} \exp\left[-\frac{(p_0^2 + \mathbf{p}_\perp^{-2})}{2\alpha^2}\right] \quad (55)$$

Similarly, from appendix A,

$$\mathcal{L}_q = a_L \partial_{p_0}^3 + a_T \partial_{p_0} \partial_{\mathbf{p}_\perp}^2 \quad (56)$$

Hence, the analytic solution is similar to the two-dimensional case on a plane defined by p_0 and p_\perp . For the stochastic time development, consider \mathcal{L}_q acting on a test point during time interval Δt . Thus,

$$\mathcal{J}(\mathbf{p} - \mathbf{p}_i) = e^{-\mathcal{L}_{q_2} \Delta t} e^{-\mathcal{L}_{q_1} \Delta t} \delta(p_0 - p_{0i}) \delta(p_1 - p_{1i}) \delta(p_2 - p_{2i}) \quad (57)$$

where \mathcal{L}_{q_1} and \mathcal{L}_{q_2} are given by equations (25) and (26), respectively. The sample set generated by \mathcal{L}_{q_1} and \mathcal{L}_{q_2} acting successively on the test point creates four new pairs to $\mathcal{O}(\Delta t)$.

The operator \mathcal{L}_{q_1} generates two sets of pairs as in the two-dimensional case that can be written succinctly as

$$\sum_{j \neq i=1}^2 \delta(p_0 - p_{0j}) \delta(p_1 - p_{1j}) \delta(p_2 - p_{2i}) \sigma_i \sigma_{j\pm}$$

Similarly, \mathcal{L}_{q_2} acting on $\delta(\mathbf{p} - \mathbf{p}_i)$ generates the set,

$$\sum_{j \neq i=1}^2 \delta(p_0 - p_{0j}) \delta(p_2 - p_{2j}) \delta(p_1 - p_{1i}) \sigma_i \sigma_{j\pm}$$

Figure 6 shows the results for the $(\mathbf{p}_0, \mathbf{p}_1)$ plane. The comparison with analytic solutions (fig. 4) is remarkably good even with 10 000 initial test points. Also, by choosing $a \Delta t = 0.01$, only 10 time steps are required.

IV. Application in Two-Dimensional Phase Space

The full quantum motion, namely the classical evolution followed by the quantum jumps, is applied to an arbitrary initial state in an anharmonic quartic potential:

$$V(x) = \frac{1}{2} (x^2 + kx^4) \quad (58)$$

Note that this potential provides an exact description of the quantum effects within the quasi-classical approximation as all higher order terms vanish. The problem is first studied in two-dimensional phase space to validate the technique with exact solutions calculable by standard numerical techniques. The power of the technique developed herein lies in its direct applicability to higher dimensions and to many-body systems.

The initial Wigner functions are chosen from a class of functions represented by

$$f(x, p, 0) = 2 \exp \left\{ -\beta \left[(x - x_0)^2 - (p - p_0)^2 \right] \right\} \quad (59)$$

such that $f_\omega = \beta f$, where the parameter β defines arbitrary admixtures of states. The examples considered have $x_0 = 0$, and $p_0 = 1$. (See fig. 7 for $\beta = 0.25$.) With $\beta = 1$, the Wigner function corresponds to a minimum wavepacket that is a pure state. (See eq. (7).) For $\beta < 1$ the function therefore describes a mixture of states. Obviously, $\beta > 1$ is not allowed because of the uncertainty relations $\Delta x \Delta p \leq \frac{1}{2}$.

The algorithm is based on the following complex of procedures using C-language. The initial set of test points is assigned to a fine mesh of phase-space grids. A list of structures is constructed, each structure containing the data corresponding to the coordinates of the grid, the density, and the sign of the test points. Only the nonempty grids form the list. For the classical motion with mass $m = 1$, the coordinate data are updated by using a two-step second-order Runge-Kutta method. This computation can be as accurate as desired and does not involve a grid approximation. A high degree of accuracy is essential for the classical motion.

To implement the quantum event, all test points within a particular region in position space having all possible momentum values are identified by sorting. (To facilitate sorting, the list is constructed at two levels. The first level, which consists of structures for a coarse x -grid, forms the main trunk. From each unit on the trunk, a branch containing all the structures that fall within that unit are attached. The second-level structures contain the actual data.) The

selected set is then allowed to undergo one-dimensional quantum jumps. (See section III.) The cumulative distribution for $F_{\pm}(a; p)$ is tabulated for various values of a . The required value of a is computed at the coarse x -grid location via $a = [V'''(x) \Delta t]/24$. The net sum of newly formed test points is attached to the main list. The entire x -space is spanned in this manner.

With low creation probabilities and the annihilation of pairs of opposite signs within the assigned grid spacing for quantum motion, the main list does not increase exponentially and remains tractable. The initial number of test points (N) was taken to be 20 000, which formed an initial list size of approximately 4000 and grew to a size of approximately 15 000 at the end of $t = 4\pi$. The enhancement factor M was chosen as $M = 5$ with the grid size (annihilation distance) set at approximately 0.3. The test points were given Gaussian width $\alpha' = 0.4$. The function is reconstructed at the required time intervals from the test points by using a suitable set of orthonormal harmonic oscillator test functions. On a micro VAX-4000 series computer (manufactured by Digital Equipment Corporation), the run time for the $0-\pi$ time segment was typically 5 minutes, but for the $0-4\pi$ time segment it was approximately 40 minutes because of the increasing list size.

An earlier version of the algorithm was written in PL/I language (ref. 10). One complicated feature of the algorithm was the task of keeping track of the four nearest neighbors of a moving sample test point in order to facilitate sorting and annihilations of the newly created pairs with their nearest neighbors having opposite signs. The algorithm developed here has proven to be faster and more accurate.

V. Results and Discussion

Snapshots of the motion at time intervals in units of π are shown in figures 8–14 for various initial Wigner functions and for various strengths of the potential. Each time unit is subdivided into 30 time steps. The results are compared both with the exact solution calculated by standard numerical techniques (ref. 10) and with the solutions of the classical Liouville equation.

The following observations can be made regarding the classical motion versus the quantum motion. For the classical motion, the volume of phase space occupied by the system (an integral invariant of Poincaré) remains constant (ref. 17), but it streams out into all phase-space regions allowed by energy conservation, with the occupied phase-space region developing whorls and tendrils. (See fig. 14.) After long intervals of time, this spread gives the appearance of a uniform distribution over a coarse grid, although finer grids would reveal the fine detail of the contour levels as they are the classical solutions shown in figures 8–14 (part (a)). For the quantum motion, however, the system maintains a cohesiveness as the unit oscillates within the potential well. This cohesion is the result of quantum interference effects arising from the oscillations of the Airy functions, thus causing cancellations and reinforcements over the classical motion.

Quantitative differences for the pure state ($\beta = 1$) and the mixed state ($\beta < 1$) quantum motions are also evident. For the pure state motion, the maximum height of the Wigner function is observed to remain unchanged. However, the mixed-state motion shows a “quantum focusing” effect as the Wigner function peaks beyond its initial maximum. Clearly, classical motion does not allow for such effects resulting from the Liouville theorem, which states that the density of systems in the neighborhood of some given system in phase space remains constant in time (ref. 17).

Finally, as an example of computation of an observable quantity, the averages of x and p are shown in figure 15, where

$$\langle x \rangle = (2\pi)^{-1} \int dx dp f_w(x, p, t) x \quad (60)$$

$$\langle p \rangle = (2\pi)^{-1} \int dx dp f_w(x, p, t) p \quad (61)$$

The averages are plotted both for the purely classical and the full quantum motion. For the classical motion, the system distributes uniformly around the equilibrium point, consistent with energy conservation, and the first moments of the distribution approach zero at late times. For the quantum motion, however, these moments are oscillatory with finite amplitude, an indication of a preservation of structural unity over long intervals of time.

Statistical fluctuations are inherent in any Monte Carlo simulation. By increasing the number of initial test points, these fluctuations can be made negligible and a single computer run then becomes sufficient for accuracy. In conclusion, the method pursued in this work shows great promise for application to multidimensional problems in which other numerical procedures may prove to be difficult.

VI. Concluding Remarks

The quantum Liouville equation in the Wigner representation is solved numerically by using Monte Carlo methods. For incremental time steps, the propagation is implemented as a classical evolution in phase space modified by a quantum correction. The correction, which is a momentum jump function, is simulated in the quasi-classical approximation via a stochastic process. In this paper the technique, which is developed and validated in two- and three-dimensional momentum space, extends an earlier one-dimensional work. Also, by developing a new algorithm, the application to bound state motion in an anharmonic quartic potential shows better agreement with exact solutions in two-dimensional phase space.

Work is well under way toward the development of a code to a six-dimensional case for application to potential scattering problems and low-energy barrier penetration. Future work will involve extensions to few-body scattering and the inclusion of quantum statistics to account for the Pauli blocking effects of spin one-half fermion systems. These are long-term projects, but a beginning has been made.

NASA Langley Research Center
Hampton, VA 23681-0001
November 23, 1993

Appendix A

Quantum Evaluation Operator

In this appendix we expand \mathcal{L}_q in terms of the radial component p_0 and the perpendicular components p_1 and p_2 of the momentum. For this we evaluate

$$Q = V(r) \left(\overleftarrow{\nabla}_{\mathbf{x}} \cdot \overleftarrow{\nabla}_{\mathbf{p}} \right)^3 \delta(\mathbf{p}) = V(r) \frac{1}{(2\pi)^3} \int \left(\overleftarrow{\nabla}_{\mathbf{x}} \cdot \mathbf{y} \right)^3 e^{i\mathbf{p} \cdot \mathbf{y}} d\mathbf{y}$$

in terms of parallel (0) and perpendicular (\perp) components to get

$$\begin{aligned} \nabla_{\mathbf{x}} &\equiv \left(\hat{e}_r \partial_r, \hat{e}_{\perp} \frac{\partial_{\perp}}{r} \right) \\ \mathbf{y} &\equiv (\hat{e}_r y_0, \hat{e}_{\perp} \mathbf{y}_{\perp}) \end{aligned}$$

Using the relations

$$\partial_{\perp} y_0 = \mathbf{y}_{\perp} \quad \partial_{\perp} \mathbf{y}_{\perp} = -y_0$$

gives

$$(\nabla_{\mathbf{x}} \cdot \mathbf{y}) V(r) = V' y_0$$

$$(\nabla_{\mathbf{x}} \cdot \mathbf{y})^2 V(r) = V'' y_0^2 + \frac{V'}{r} \mathbf{y}_{\perp}^2$$

$$(\nabla_{\mathbf{x}} \cdot \mathbf{y})^3 V(r) = V''' y_0^3 + 3 \partial_r \left(\frac{V'}{r} \right) y_0 \mathbf{y}_{\perp}^2$$

$$Q = \frac{1}{(2\pi)^3} \int \left[V''' y_0^3 + 3 \partial_r \left(\frac{V'}{r} \right) y_0 \mathbf{y}_{\perp}^2 \right] e^{i\mathbf{p} \cdot \mathbf{y}} d\mathbf{y} = \left[V''' \partial_{p_0}^3 + 3 \partial_r \left(\frac{V'}{r} \right) \partial_{p_0} \partial_{\mathbf{p}_{\perp}}^2 \right] \delta(\mathbf{p})$$

Hence,

$$\mathcal{L}_q = \frac{1}{24} \left[V''' \partial_{p_0}^3 + 3 \partial_r \left(\frac{V'}{r} \right) \partial_{p_0} \partial_{\mathbf{p}_{\perp}}^2 \right]$$

Appendix B

Expressions for Modified Airy Functions \mathcal{J}_α

Expressions for the damped Airy functions are obtained in this appendix. The expression to be evaluated is

$$\mathcal{J}_\alpha(a; p) = e^{-a\partial_p^3} \delta_\alpha(p)$$

where

$$\delta_\alpha(p) = \frac{1}{\sqrt{2\pi\alpha}} e^{-p^2/2\alpha^2}$$

The results are presented here. For details, see reference 10 where the evaluation is done by using the method of steepest descent (ref. 18).

Series Expansion for $a \ll 1$

Using the series expansion for $e^{-a\partial_p^3}$ and applying the Rodrigues formula gives

$$\mathcal{J}_\alpha(a; p) = \delta_\alpha(p) \sum_n \frac{a^n}{n! (\sqrt{2}\alpha)^{3n}} H_{3n} \left(\frac{p}{\sqrt{2}\alpha} \right)$$

where H is the Hermite polynomial.

Asymptotic Evaluation for $p \rightarrow \infty$

If the aforementioned expression is rewritten using the integral representation for a Gaussian function

$$\delta_\alpha(p) = \frac{1}{\sqrt{2\pi\alpha}} \int_{-\infty}^{\infty} dy \exp \left(\frac{i\sqrt{2}py}{\alpha - y^2} \right)$$

the result is

$$\mathcal{J}_\alpha(a; p) = \text{Re} \frac{\sqrt{2|p'|}}{\pi\alpha} \int_0^\infty dy \exp \left[|p'|^{3/2} \left(ia'y^3 - \frac{y^2}{\sqrt{|p'|}} \pm iy \right) \right]$$

where

$$p' = \left(\frac{\sqrt{2}}{\alpha} \right) p \quad a' = \left(\frac{\sqrt{2}}{\alpha} \right)^3 a$$

The integral is evaluated by the method of steepest descent in the complex plane. If we define

$$f(z) = ia'z^3 - \frac{z^2}{\sqrt{|p'|}} \pm iz$$

where z is a complex number, the saddle points occur at

$$z_0 = \frac{-2i}{6a'\sqrt{|p'|}} \left[1 \pm (1 + 3a'p')^{1/2} \right]$$

The integral is evaluated independently along different paths for two cases, and the resulting expressions are given as follows:

For $1 + 3a'p' > 0$,

$$\mathcal{J}_\alpha(a; p) = \operatorname{Re} \frac{1}{\sqrt{2}\pi\alpha} \exp \left[|p'|^{3/2} f(z_0) \right] \sum_{n=0}^{\infty} \frac{(ia')^n \Gamma[(3n+1)/2]}{n! |1 + 3a'p'|^{(3n+1)/4}}$$

For $1 + 3a'p' < 0$,

$$\mathcal{J}_\alpha(a; p) = \operatorname{Re} \frac{\sqrt{2}}{\pi\alpha} \exp \left[|p'|^{3/2} f(z_0) + \frac{i\pi}{4} \right] \sum_{n \text{ even}=0}^{\infty} \frac{(ia'e^{3i\pi/4})^n \Gamma[(3n+1)/2]}{n! |1 + 3a'p'|^{(3n+1)/4}}$$

In the region $(1 + 3a'p') \approx 0$ with $3a'p' < 0$, the resulting expressions are given as follows:

For $1 + 3a'p' > 0$,

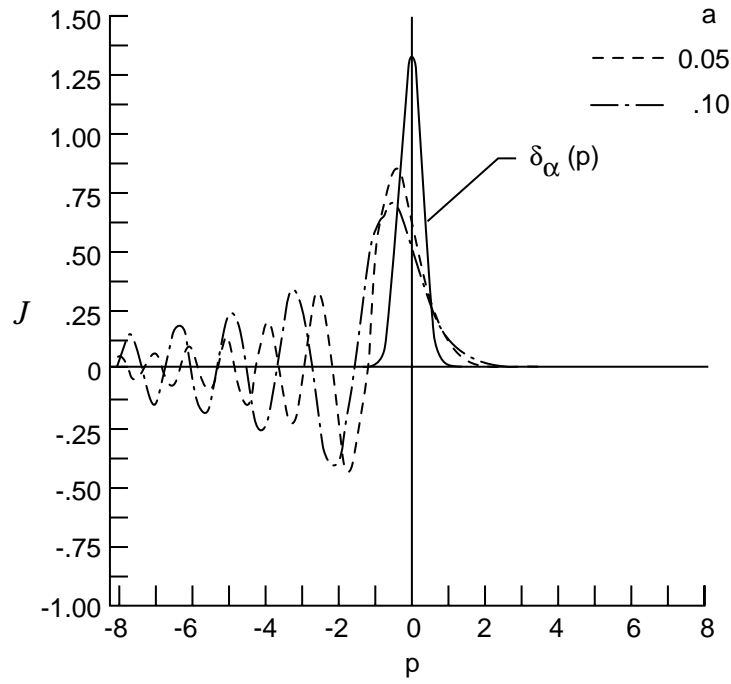
$$\mathcal{J}_\alpha(a; p) = \operatorname{Re} \frac{\sqrt{2}}{3\pi\alpha} \exp \left[|p'|^{3/2} f(z_0) + \frac{i\pi}{6} \right] \sum_{n=0}^{\infty} \frac{[-(1 + 3a'p')^{1/2} e^{i\pi/3}]^n \Gamma[(2n+1)/3]}{n! a'^{(2n+1)/3}}$$

For $1 + 3a'p' < 0$,

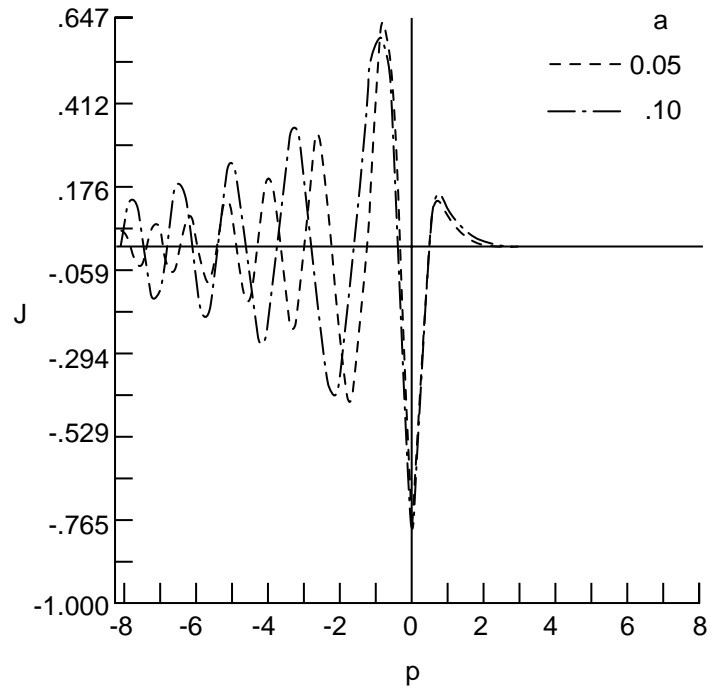
$$\begin{aligned} \mathcal{J}_\alpha(a; p) = & \operatorname{Re} \frac{\sqrt{2}}{3\pi\alpha} \exp \left[|p'|^{3/2} f(z_0) \right] \sum_{n=0}^{\infty} \frac{(1 + 3a'p')^{n/2} \Gamma[(2n+1)/3]}{n! a'^{(2n+1)/3}} \\ & \times \left\{ \exp \left[i \left(n + \frac{1}{2} \right) \frac{\pi}{3} \right] + \exp \left[i \left(n + \frac{1}{2} \right) \pi \right] \right\} \end{aligned}$$

References

1. Joachain, Charles J.: *Quantum Collision Theory*, Third ed. Elsevier Science Publ. Co. Inc., 1983.
2. Wilson, John W.; Townsend, Lawrence W.; Schimmerling, Walter; Khandelwal, Govind S.; Khan, Ferdous; Nealy, John E.; Cucinotta, Francis A.; Simonsen, Lisa C.; Shinn, Judy L.; and Norbury, John W.: *Transport Methods and Interaction for Space Radiations*. NASA RP-1257, 1991.
3. Fano, U.: Description of States in Quantum Mechanics by Density Matrix and Operator Techniques. *Reviews Modern Phys.*, vol. 29, no. 1, Jan. 1957, pp. 74–93.
4. Wigner, E.: On the Quantum Correction for Thermodynamic Equilibrium. *Phys. Review*, vol. 40, June 1, 1932, pp. 749–759.
5. Carruthers, P.; and Zachariasen, F.: Quantum Collision Theory With Phase-Space Distributions. *Reviews Modern Phys.*, vol. 55, no. 1, Jan. 1983, pp. 245–285.
6. Imre, Kaya; Özizmir, Ercüment; Rosenbaum, Marcos; and Zweifel, P. F.: Wigner Method in Quantum Statistical Mechanics. *J. Math. Phys.*, vol. 8, no. 5, May 1967, pp. 1097–1108.
7. Remler, E. A.: Use of the Wigner Representation in Scattering Problems. *Ann. Phys.*, vol. 95, 1975, pp. 455–459.
8. Nix, J. R.; and Strottman, D.: Effect of a Density Isomer on High-Energy Heavy-Ion Collisions. *Phys. Review C*, vol. 23, no. 6, June 1981, pp. 2548–2556.
9. Bertini, Hugo W.: Intranuclear-Cascade Calculation of the Secondary Nucleon Spectra From Nucleon-Nucleus Interactions in the Energy Range 340 to 2900 MeV and Comparisons With Experiment. *Phys. Review, second ser.*, vol. 188, no. 4, Dec. 20, 1969, pp. 1711–1730.
10. John, Sarah: Solution to Quantum Liouville Equation in Phase Space Via a Stochastic Process. Ph.D. Diss., College of William and Mary, 1986.
11. John, Sarah; and Remler, E. A.: Solution of the Quantum Liouville Equation as a Stochastic Process. *Ann. Phys.*, vol. 180, 1987, pp. 152–165.
12. Smith, T. B.: Path Sums for Brownian Motion and Quantum Mechanics. *Physica*, vol. 100A, 1980, pp. 153–166.
13. Berry, M. V.; and Balazs, N. L.: Evolution of Semiclassical Quantum States in Phase Space. *J. Phys. A: Math. Gen.*, vol. 12, no. 5, 1979, pp. 625–642.
14. Lill, J. V.; Haftel, M. I.; and Herling, G. H.: Semiclassical Limits in Quantum-Transport Theory. *Phys. Review A*, vol. 39, no. 11, June 1, 1989, pp. 5832–5841.
15. Heller, Eric J.: Wigner Phase Space Method: Analysis for Semiclassical Applications. *J. Chem. Phys.*, vol. 65, no. 4, Aug. 15, 1976, pp. 1289–1298.
16. Heller, Eric J.: Phase Space Interpretation of Semiclassical Theory. *J. Chem. Phys.*, vol. 67, no. 7, Oct. 1, 1977, pp. 3339–3351.
17. Goldstein, Herbert: *Classical Mechanics*. Addison-Wesley Publ. Co., Inc., 1950.
18. Bender, Carl M.; and Orszag, Steven A.: *Advanced Mathematical Methods for Scientists and Engineers*. McGraw-Hill Book Co., 1978.



(a) Damped Airy function $J_\alpha(a; p)$.



(b) Corresponding jump function $J_\alpha(a; p)$.

Figure 1. Typical Gaussian-modified Airy function and corresponding quantum jump function for $a = 0.05$ and 0.1 and $\alpha = 0.3$.

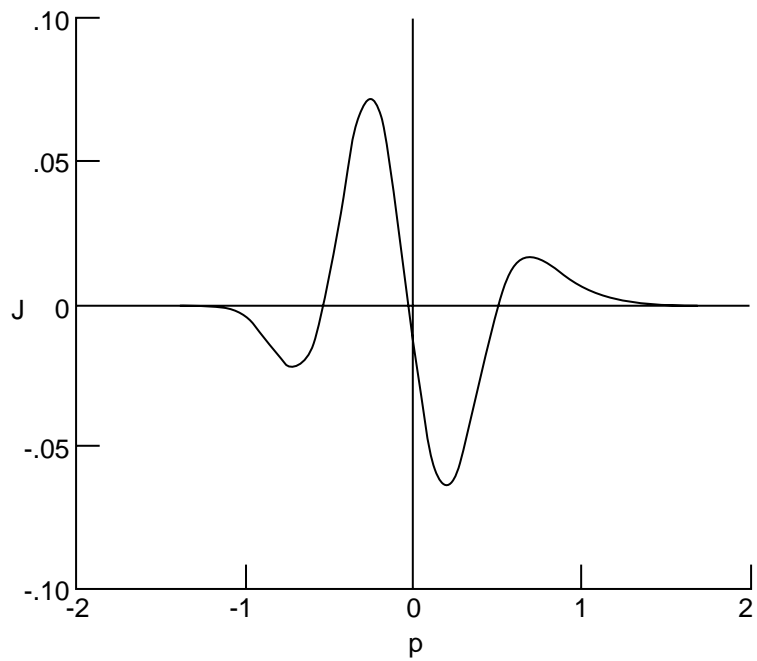
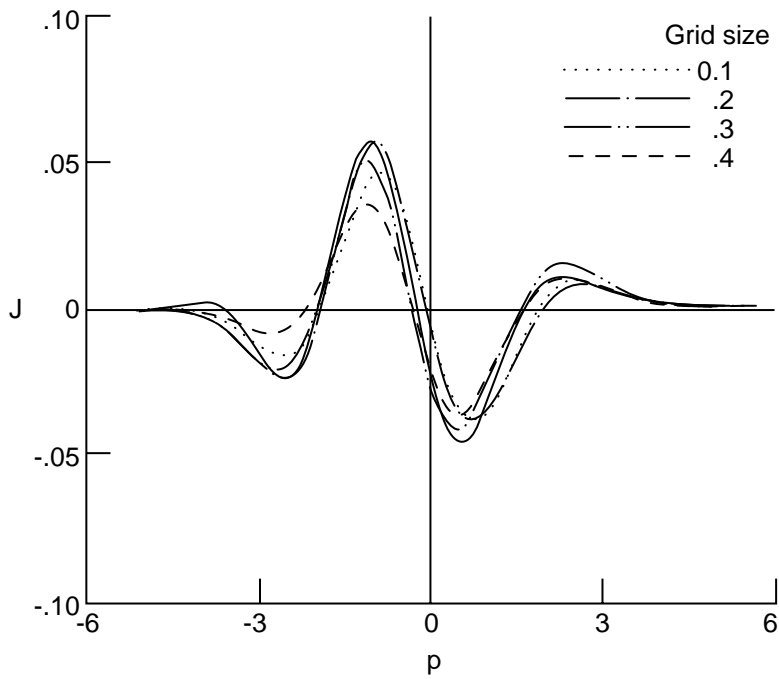
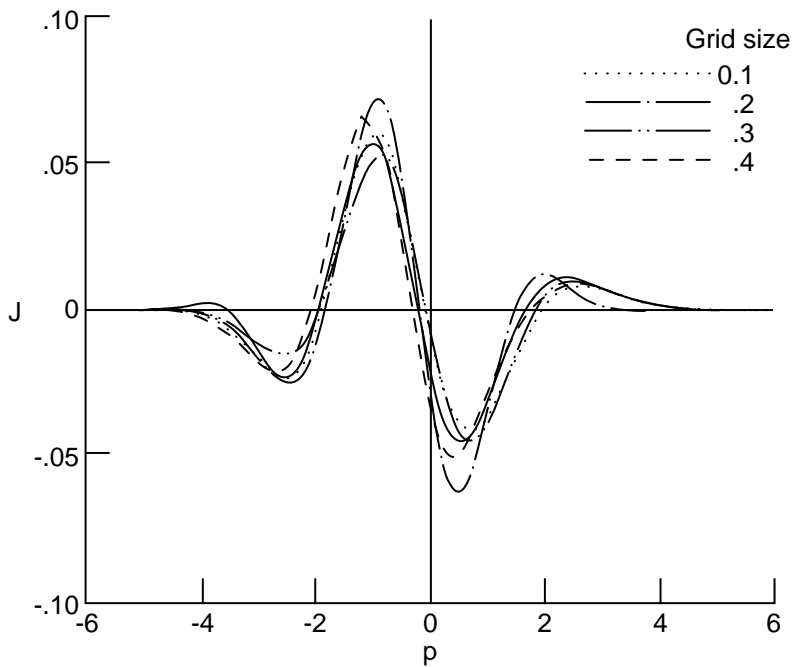


Figure 2. Jump function $J_\alpha(a;p)$ for very small increments of time for $a = 0.001$ and $\alpha = 0.3$.

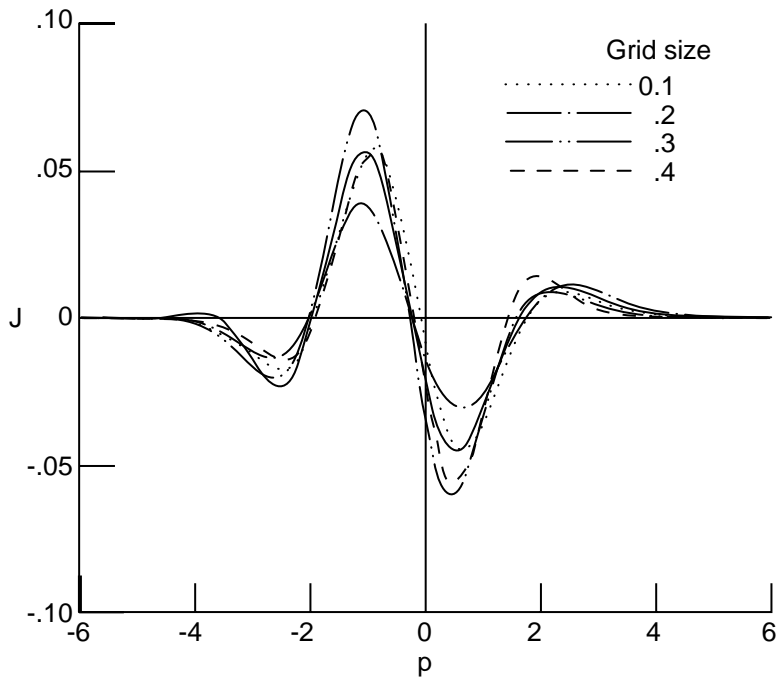


(a) $N = 100$; $\alpha' = 0.3$.

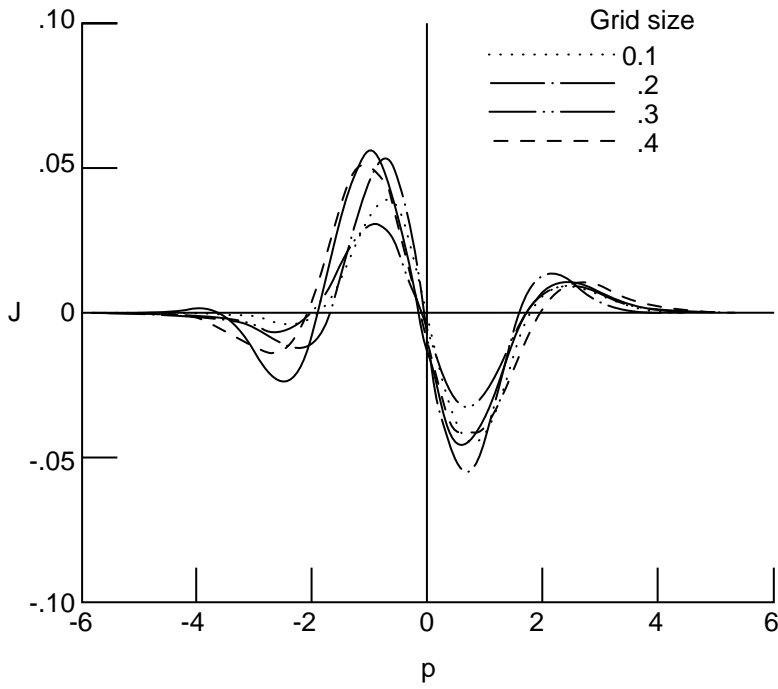


(b) $N = 10\,000$; $\alpha' = 0.3$.

Figure 3. Stochastic evolution of jump function $J_\alpha(a;p)$ after 100 time steps compared with analytic solution (solid line) at $a = 0.1$ and $\alpha = 1$ for various grid sizes.

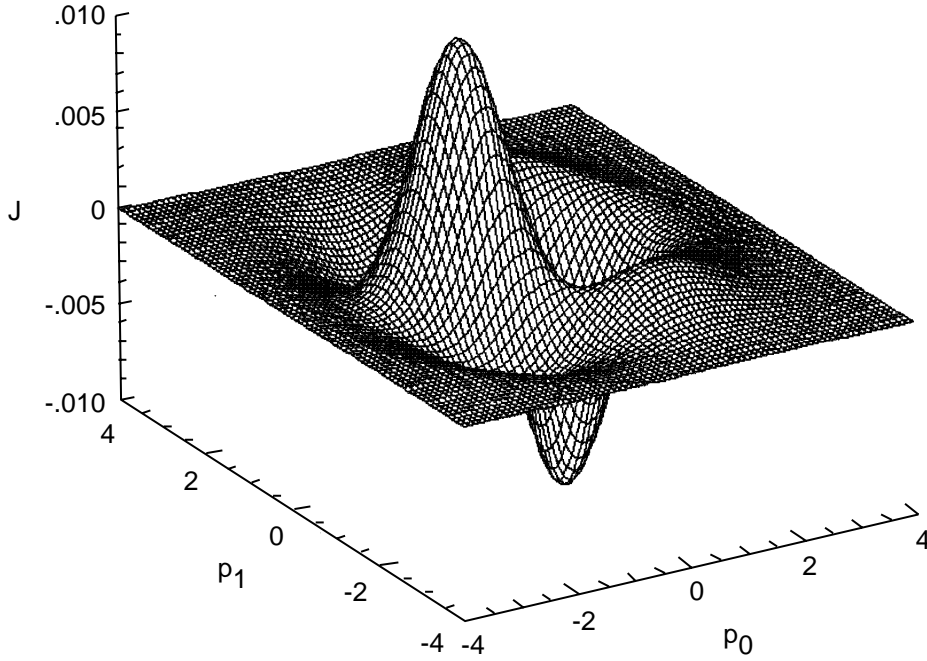


(c) $N = 1000$; $\alpha' = 0.3$.

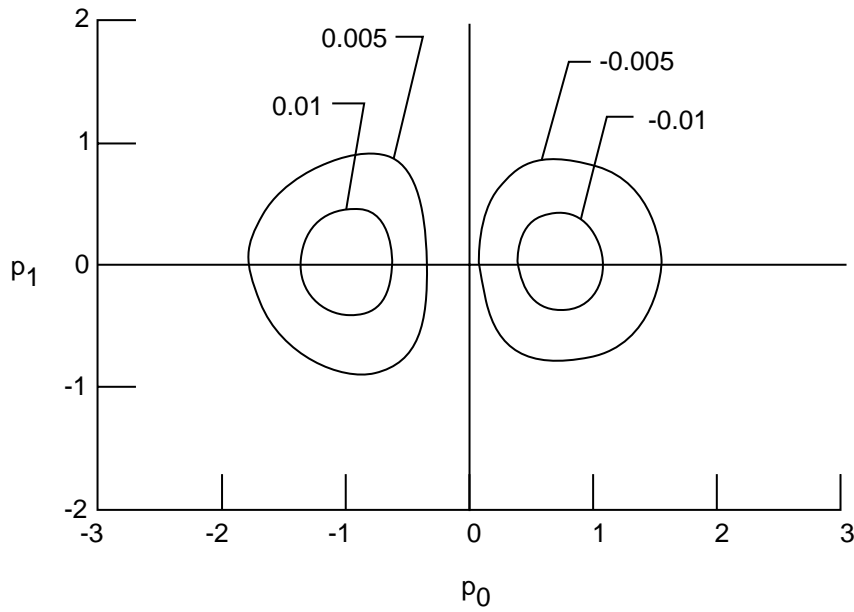


(d) $N = 1000$; $\alpha' = 0.4$.

Figure 3. Concluded.

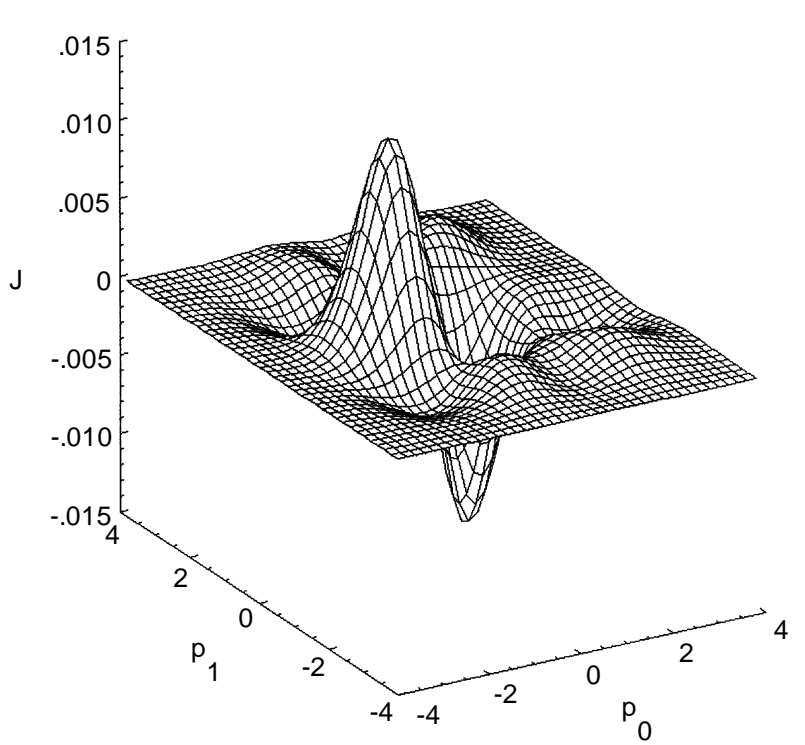


(a) Spatial representation.

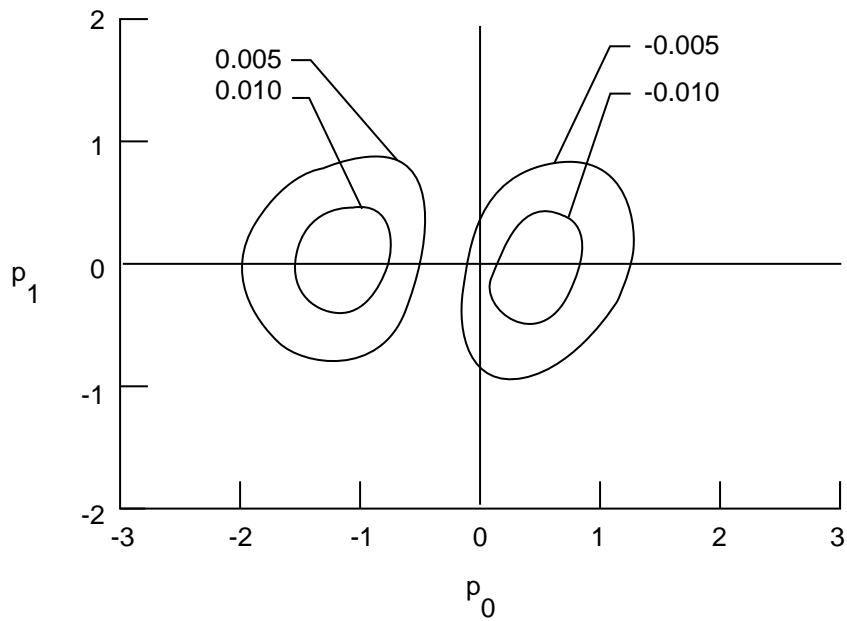


(b) Contour plot.

Figure 4. Analytic two-dimensional jump function $J_\alpha(a; p_0, p_1)$ for $a = 0.1$ and $\alpha = 1$.

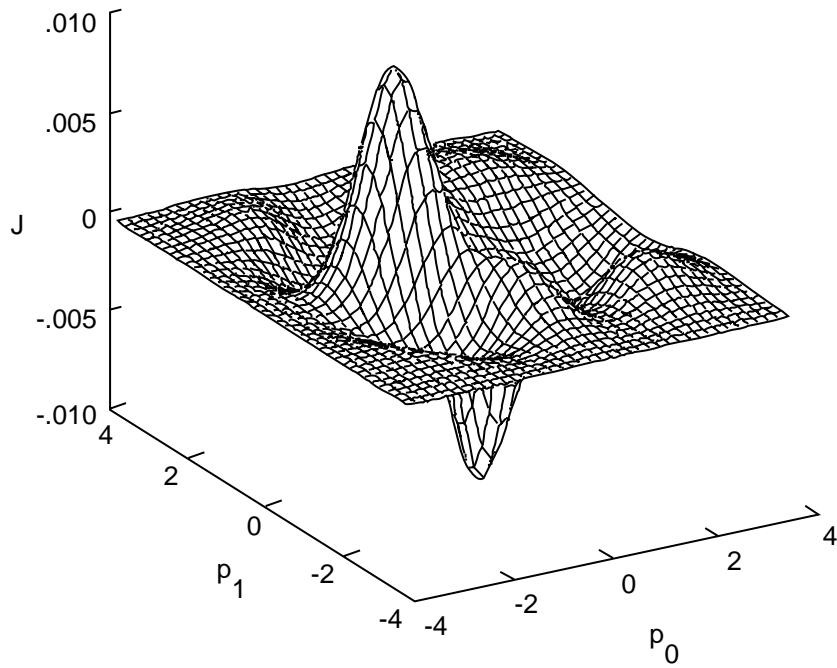


(a) Spatial representation for $N = 10\,000$, Grid size = 0.2, and $\alpha' = 0.3$.

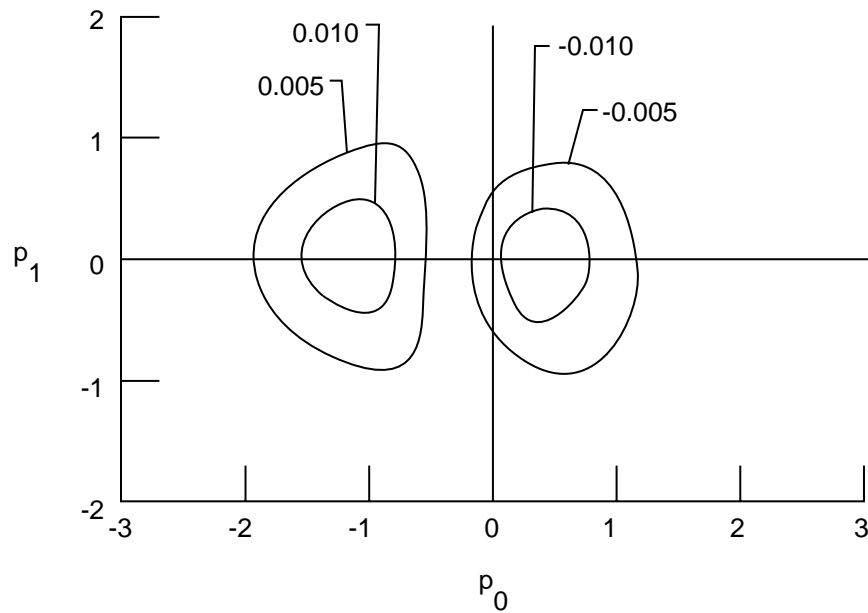


(b) Contour plot of figure 5(a).

Figure 5. Stochastic evolution of two-dimensional jump function $J_\alpha(a; p_0, p_1)$ for $a = 0.1$ and $\alpha = 1$ using 100 time steps.

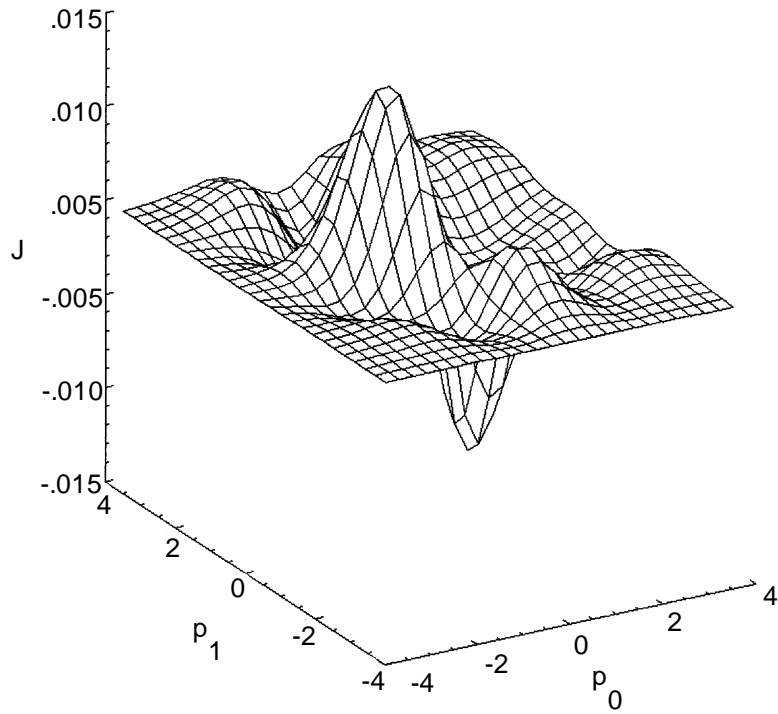


(c) Spatial representation for $N = 10\,000$, Grid size = 0.2, and $\alpha' = 0.4$.

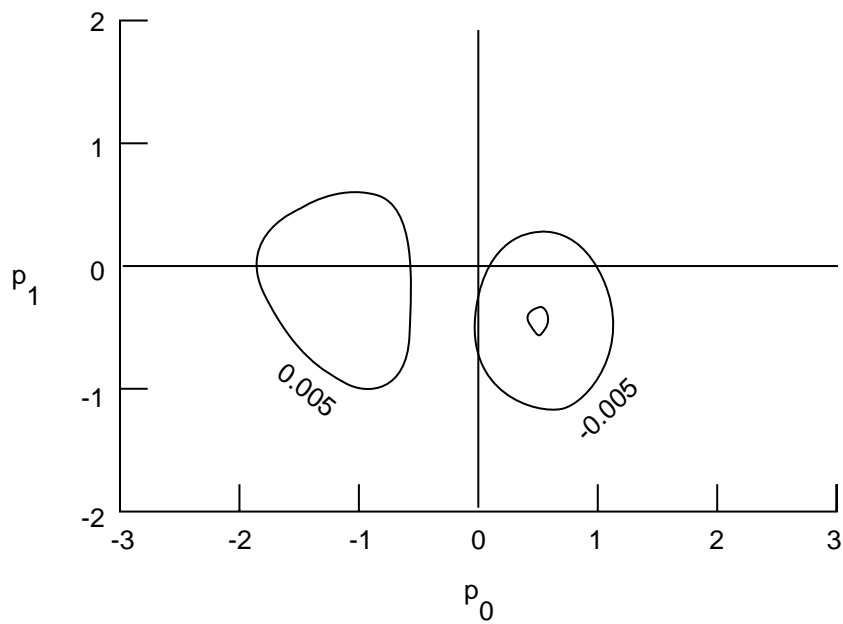


(d) Contour plot of figure 5(c).

Figure 5. Continued.

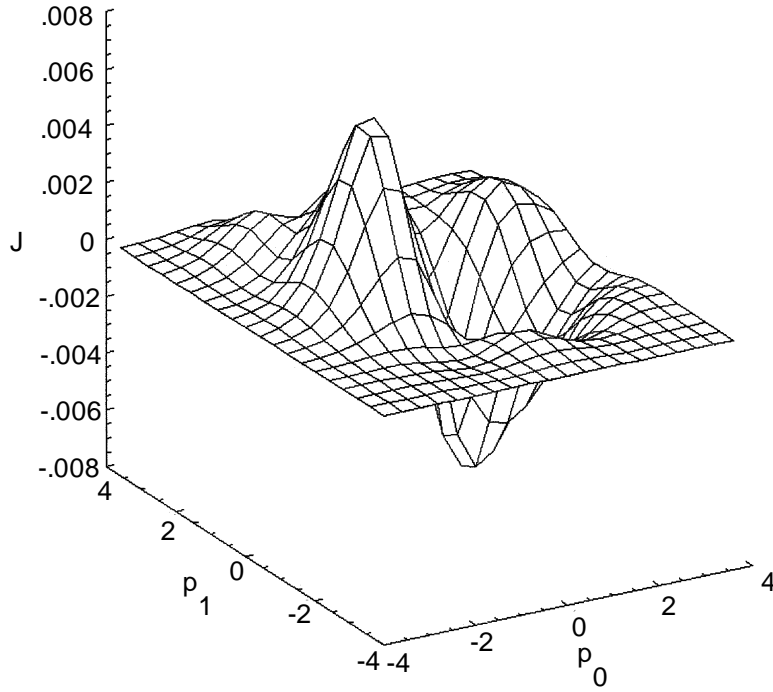


(e) Spatial representation for $N = 5000$, Grid size = 0.3, and $\alpha' = 0.3$.

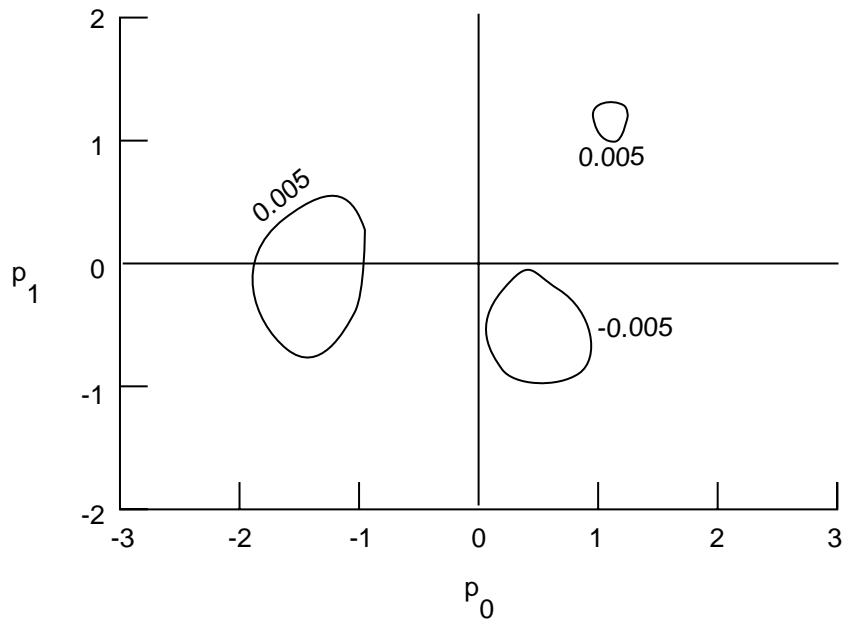


(f) Contour plot of figure 5(e).

Figure 5. Concluded.

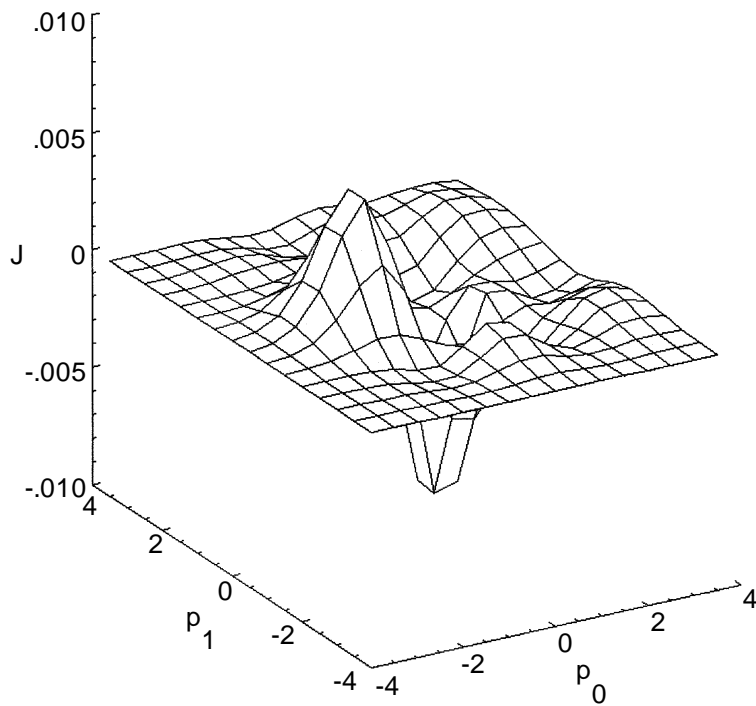


(a) Spatial representation for $N = 10\,000$, Grid size = 0.4, and $\alpha' = 0.4$.

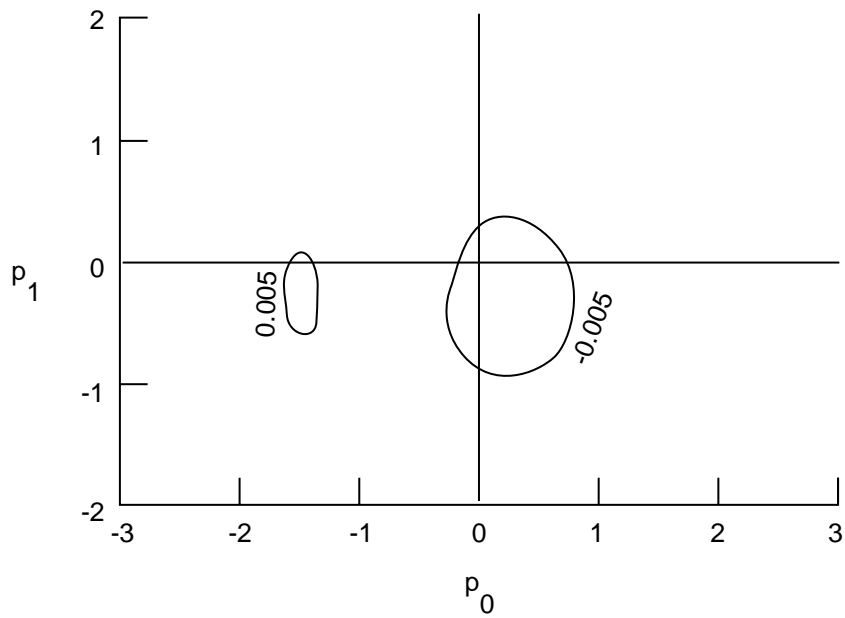


(b) Contour plot for figure 6(a).

Figure 6. Stochastic evolution of three-dimensional jump function $J_\alpha(a; \mathbf{p})$ for $a = 0.1$ and $\alpha = 1$ using 10 time steps. The plot is for the (p_0, p_1) plane.

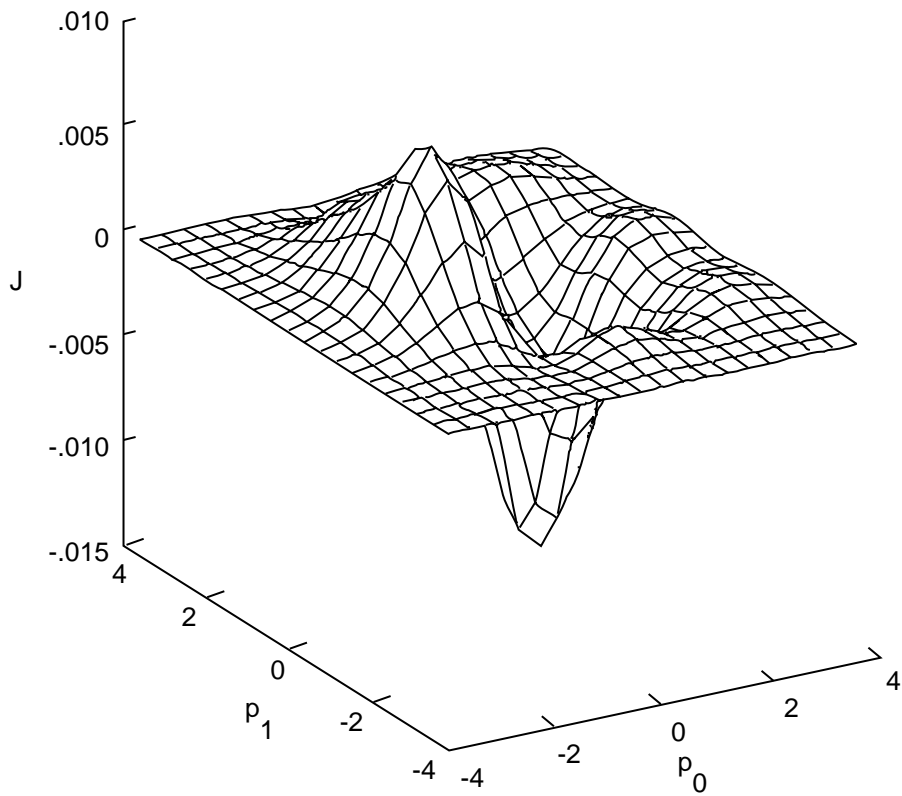


(c) Spatial representation for $N = 10\,000$, Grid size = 0.5, and $\alpha' = 0.4$.

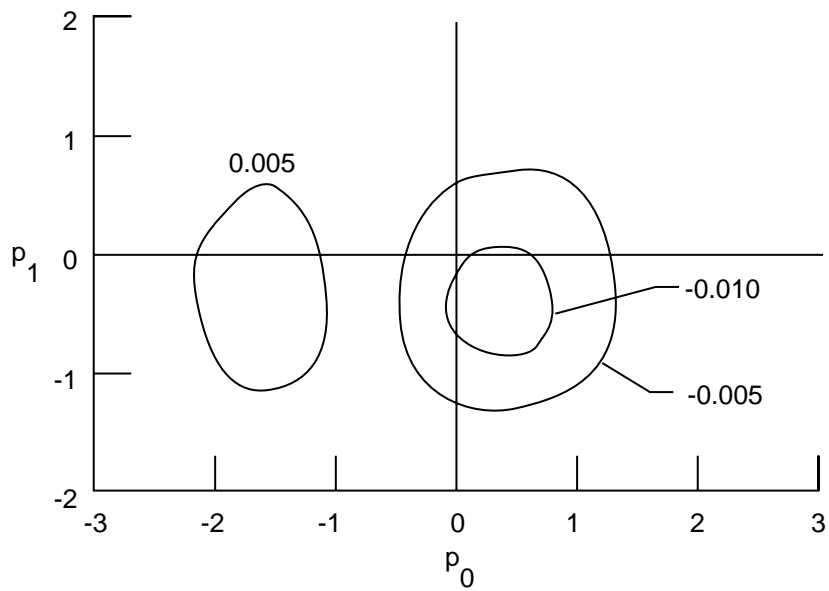


(d) Contour plot for figure 6(c).

Figure 6. Continued.

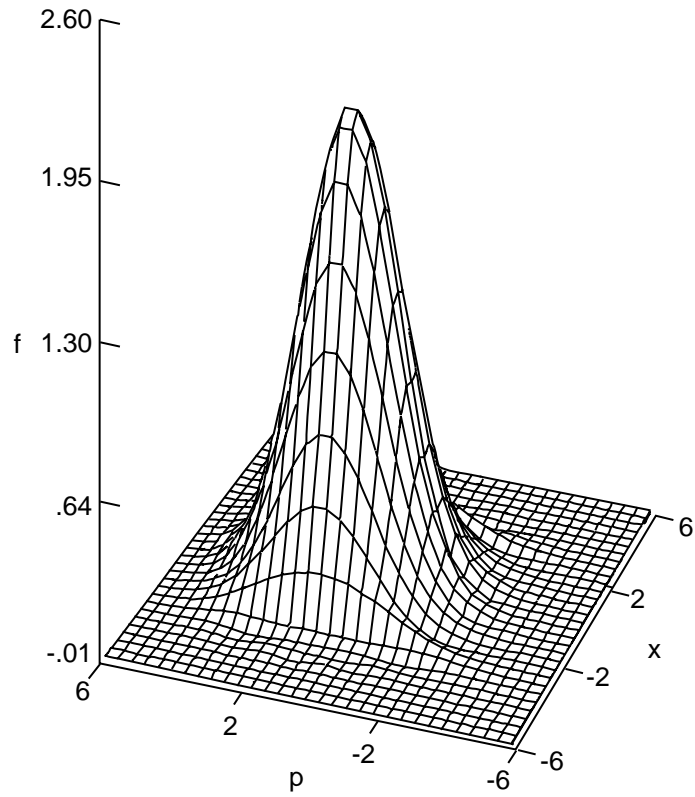


(e) Spatial representation for $N = 10\,000$, Grid size = 0.4, and $\alpha' = 0.3$.

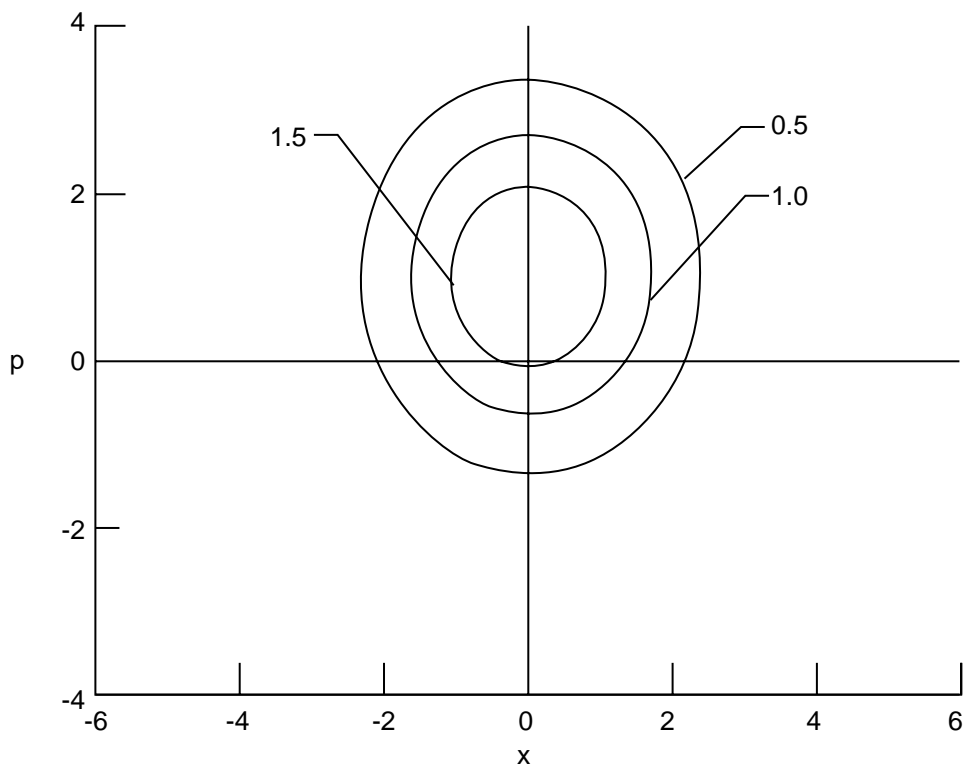


(f) Contour plot for figure 6(e).

Figure 6. Concluded.

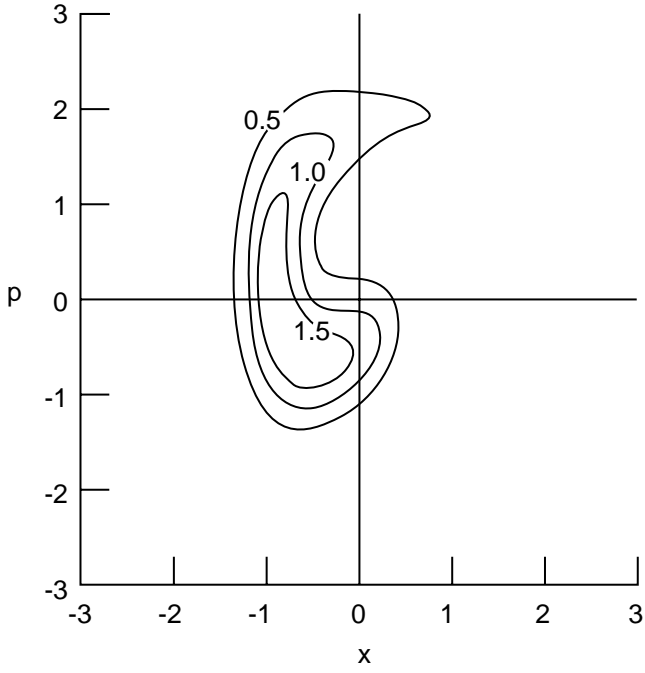


(a) Spatial representation.

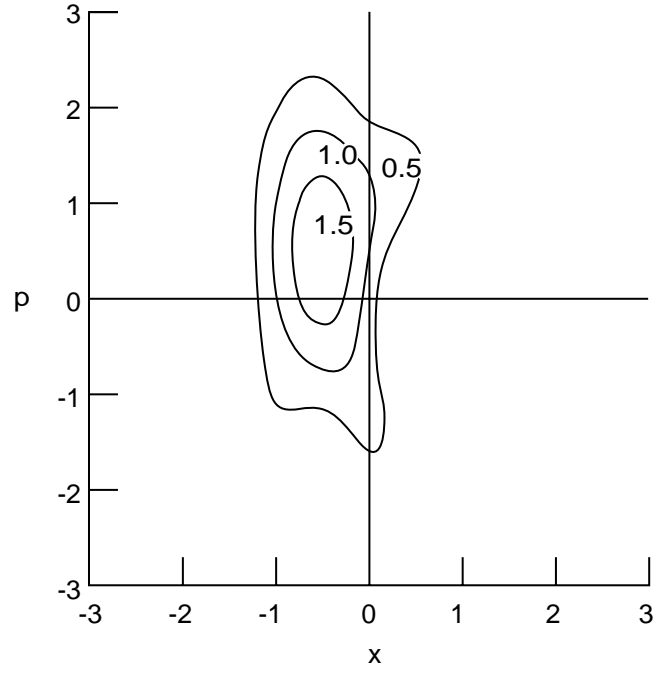


(b) Contour plot at levels of 0.5, 1.0, and 1.5.

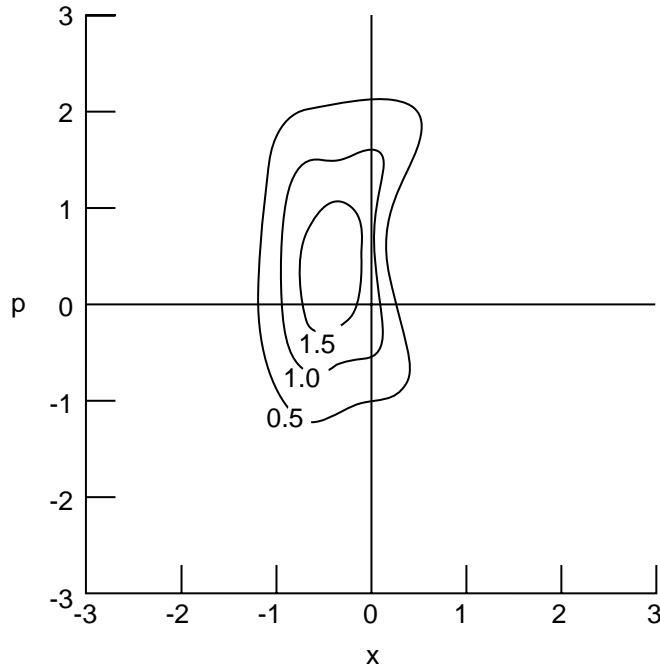
Figure 7. Values of f distribution for $\beta = 0.25$.



(a) Classical motion.

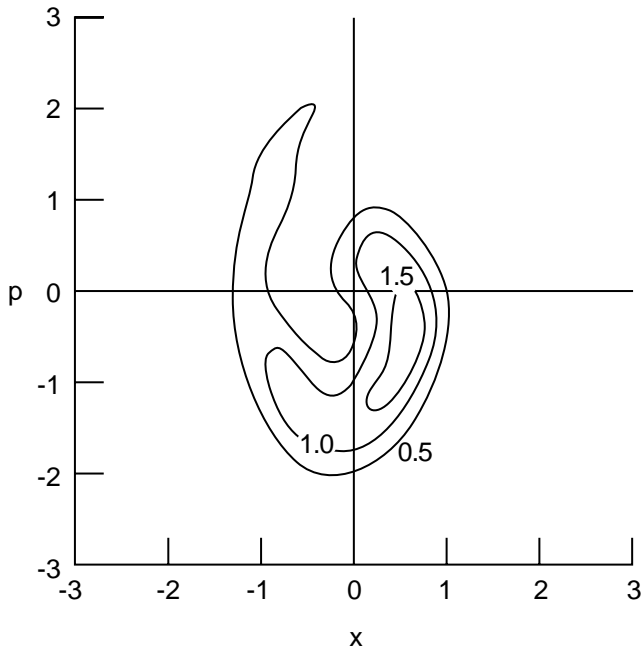


(b) Exact quantum motion.

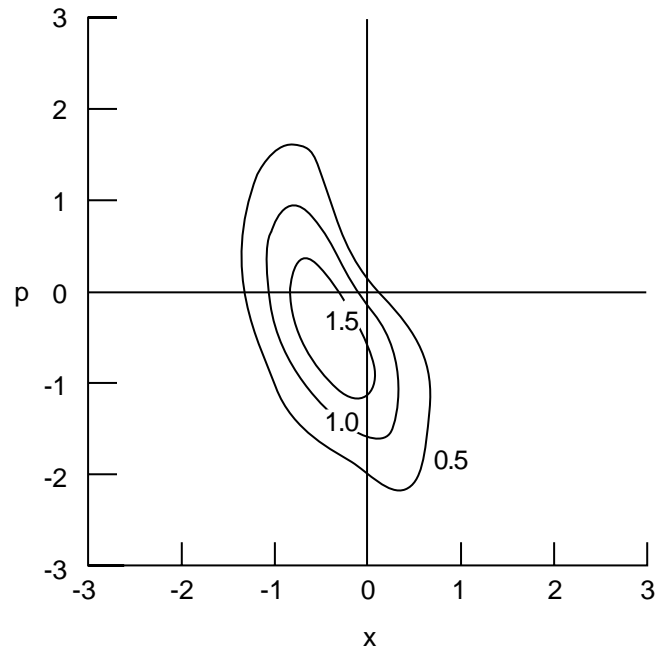


(c) Monte Carlo simulation.

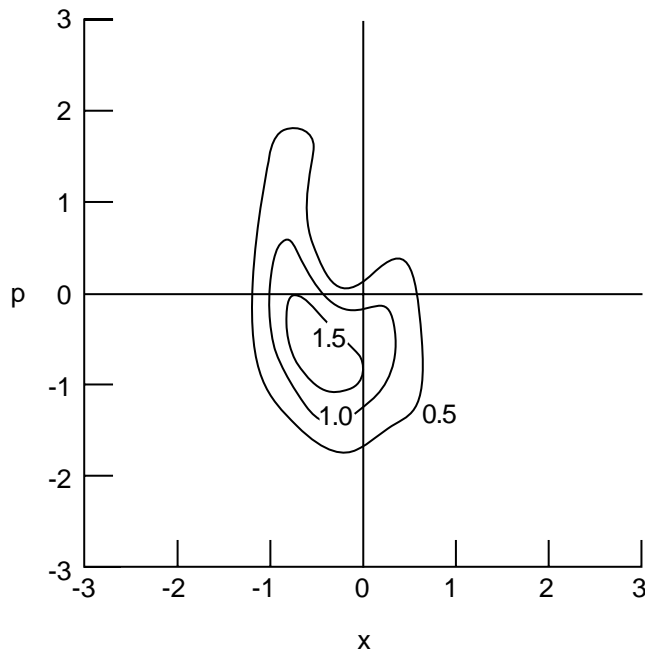
Figure 8. Contour plots of f_ω/β at levels of 0.5, 1.0, and 1.5 for $\beta = 1$, $k = 1$, Grid size = 0.3, and $\alpha' = 0.3$ at $t = \pi$ for a pure state. The symbols x and p denote the position and momentum coordinates, respectively.



(a) Classical motion.

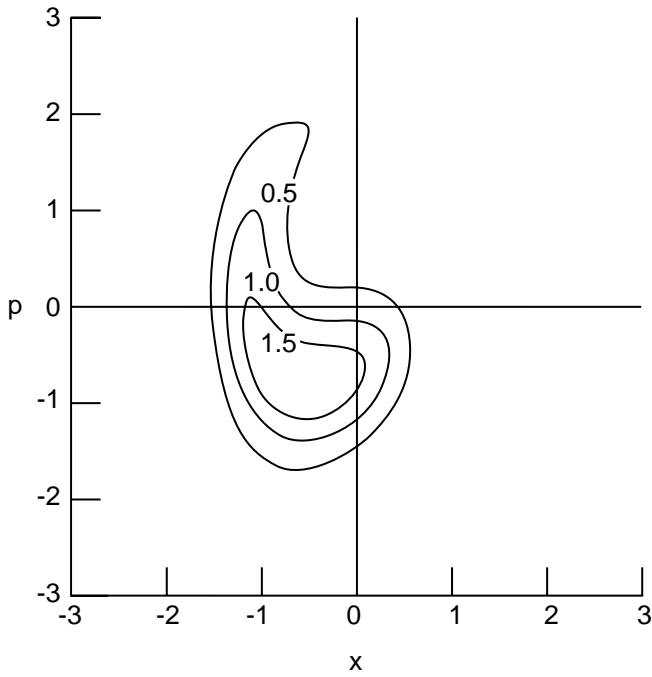


(b) Exact quantum motion.

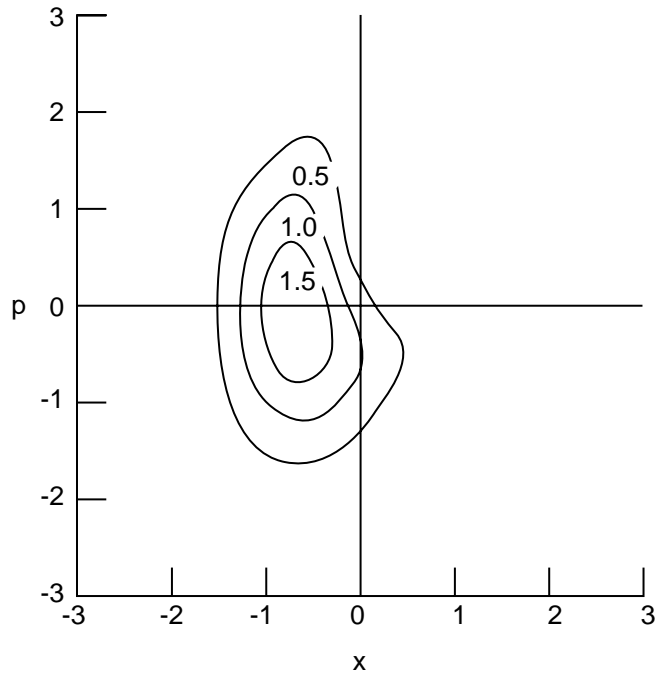


(c) Monte Carlo simulation.

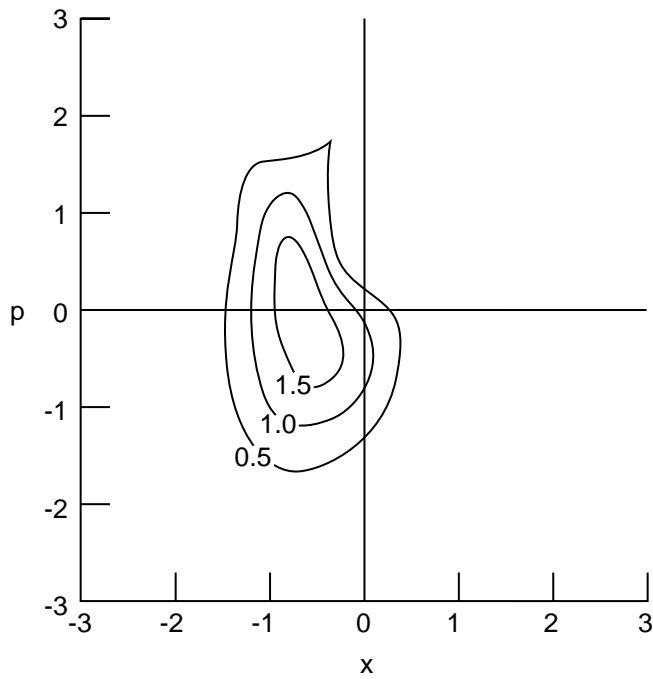
Figure 9. Contour plots of f_ω/β at levels of 0.5, 1.0, and 1.5 for $\beta = 1$, $k = 1$, Grid size = 0.3, and $\alpha' = 0.3$ at $t = 2\pi$ for a pure state. The symbols x and p denote the position and momentum coordinates, respectively.



(a) Classical motion.

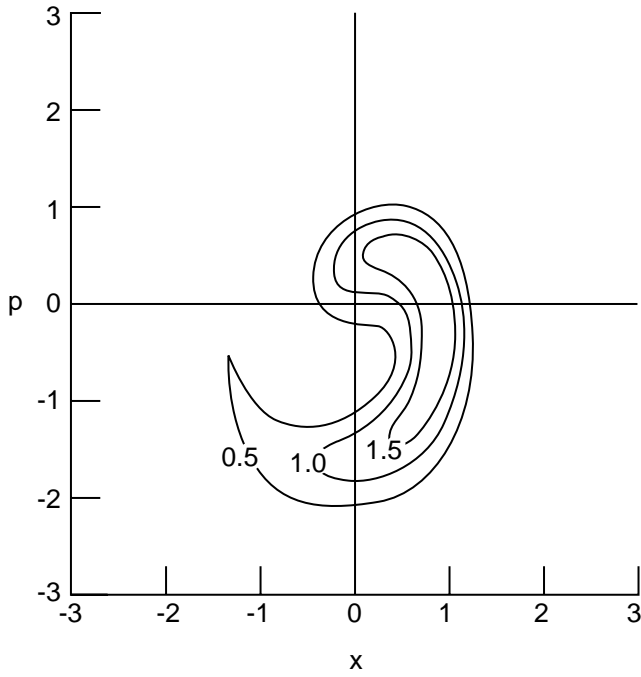


(b) Exact quantum motion.

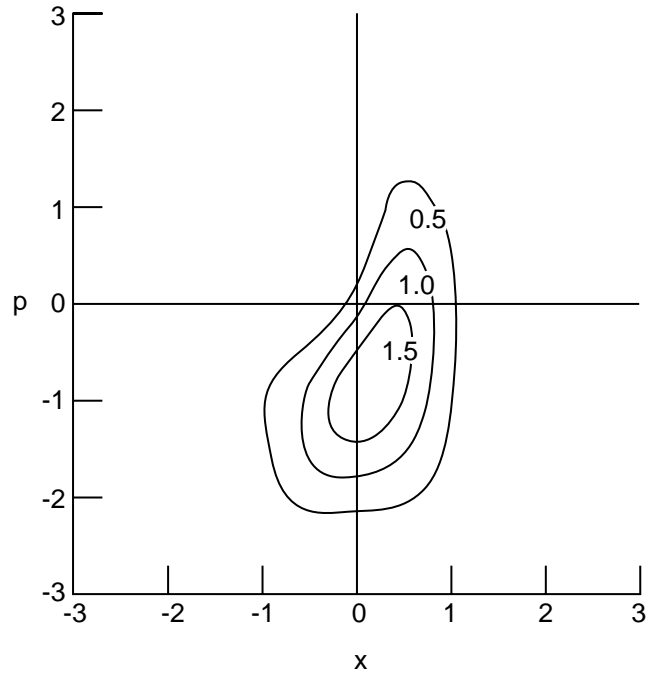


(c) Monte Carlo simulation.

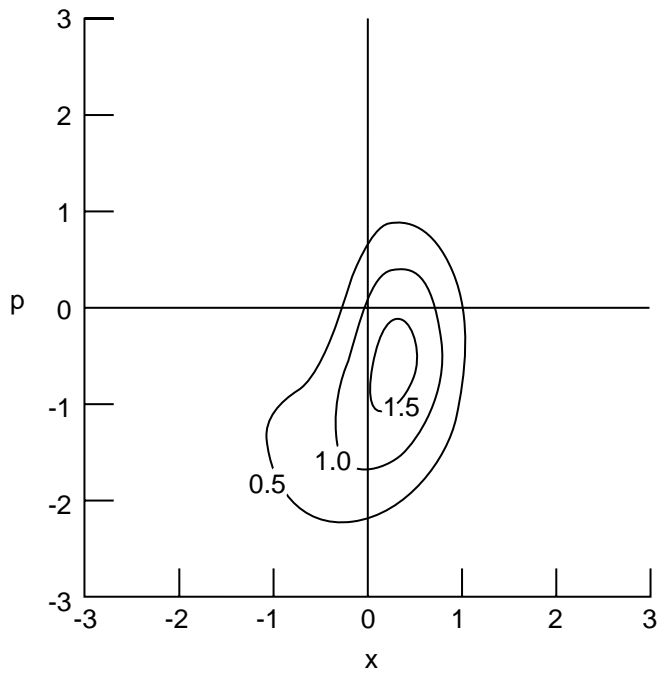
Figure 10. Contour plots of f_ω/β at levels of 0.5, 1.0, and 1.5 for $\beta = 1$, $k = 0.5$, Grid size = 0.3, and $\alpha' = 0.3$ at $t = \pi$ for a weaker potential. The symbols x and p denote the position and momentum coordinates, respectively.



(a) Classical motion.

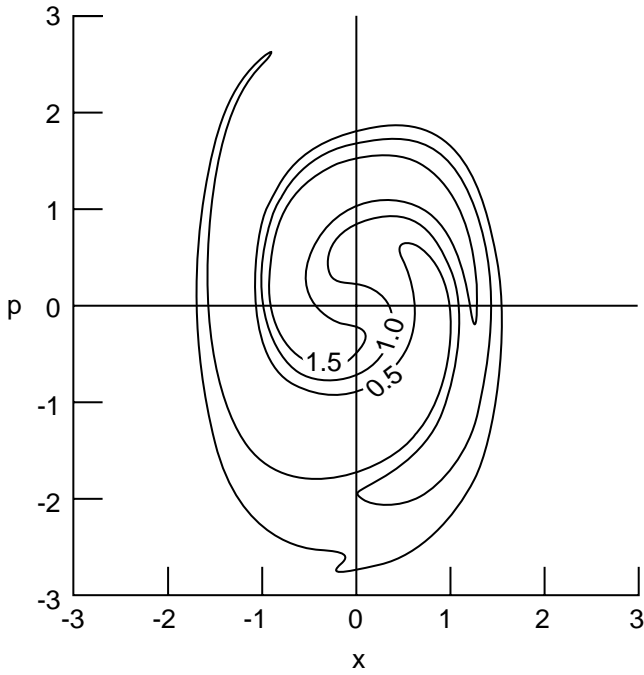


(b) Exact quantum motion.

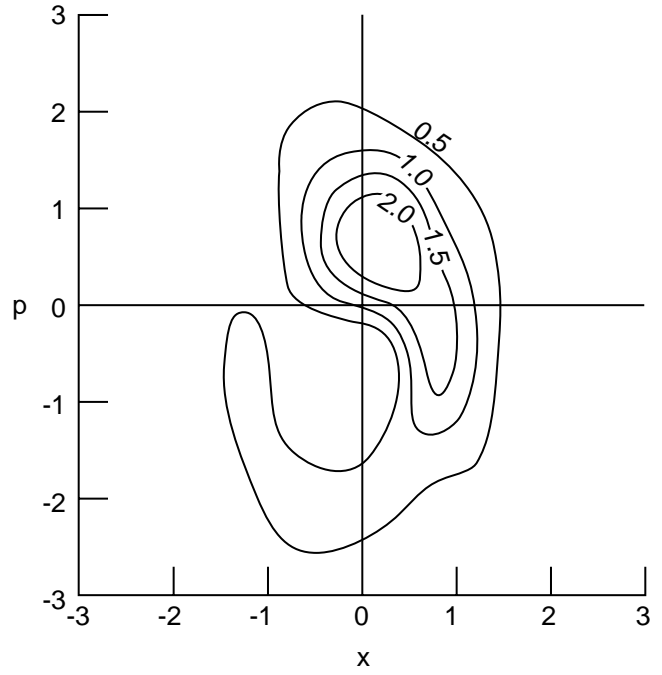


(c) Monte Carlo simulation.

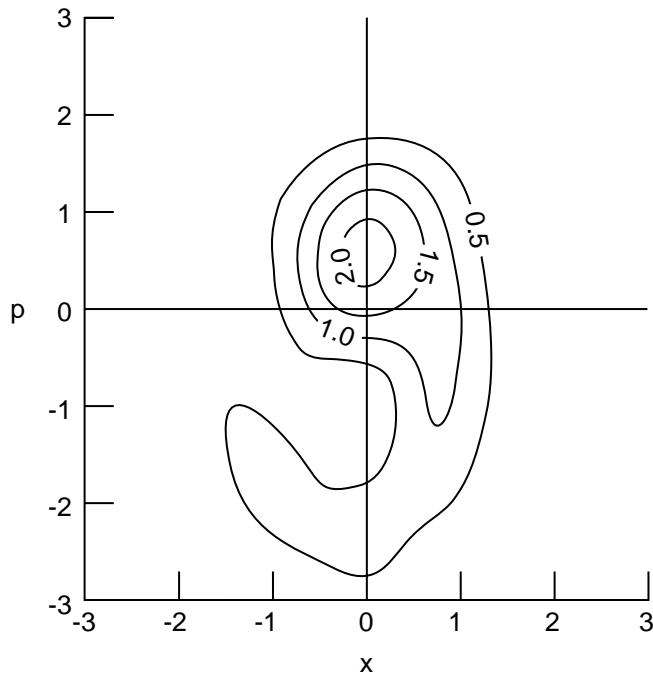
Figure 11. Contour plots of f_ω/β at levels of 0.5, 1.0, and 1.5 for $\beta = 1$, $k = 0.5$, Grid size = 0.3, and $\alpha' = 0.3$ at $t = 2\pi$ for a weaker potential. The symbols x and p denote the position and momentum coordinates, respectively.



(a) Classical motion.

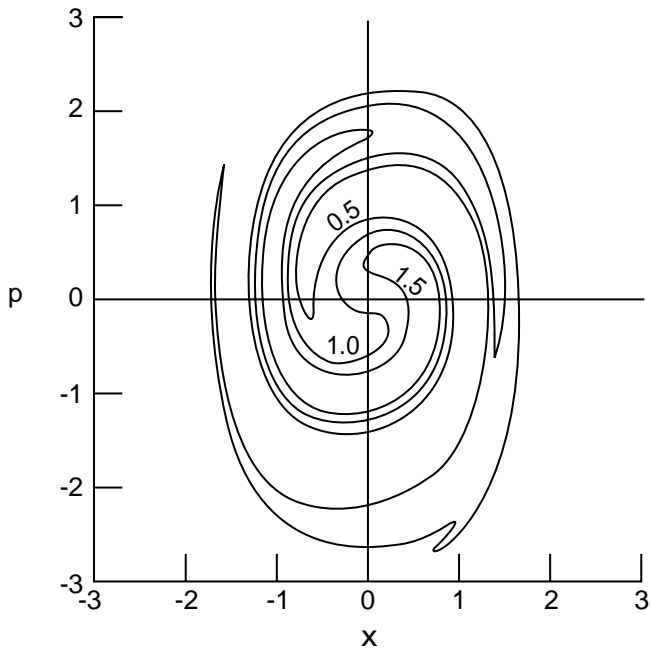


(b) Exact quantum motion.

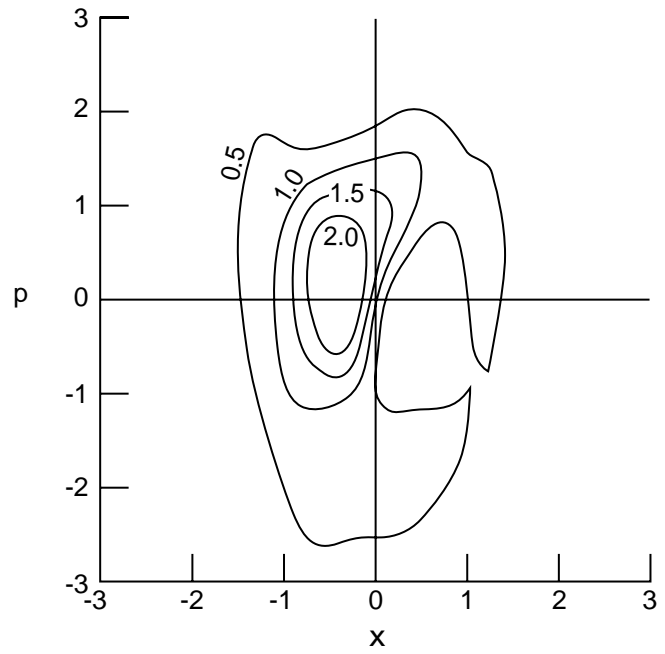


(c) Monte Carlo simulation.

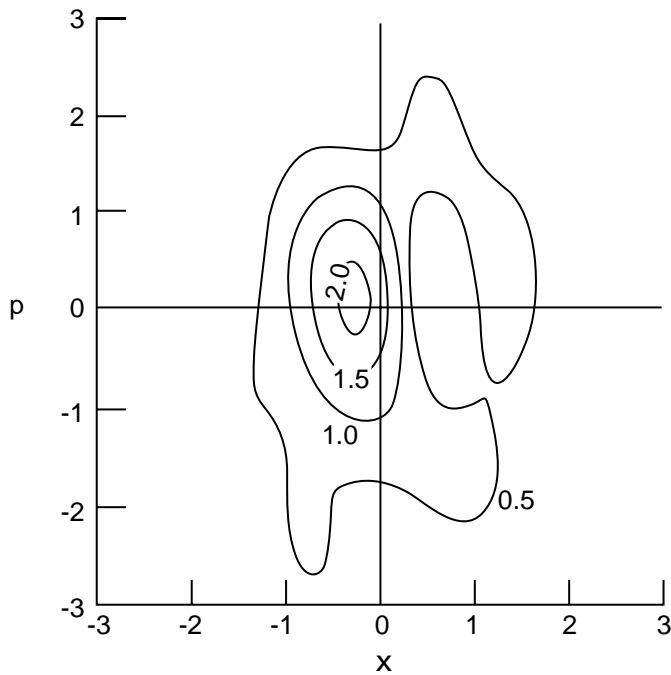
Figure 12. Contour plots of f_ω/β at levels of 0.5, 1.0, and 1.5 for $\beta = 0.5$, $k = 0.5$, Grid size = 0.3, and $\alpha' = 0.3$ at $t = 3\pi$ for a mixed state. The symbols x and p denote the position and momentum coordinates, respectively.



(a) Classical motion.

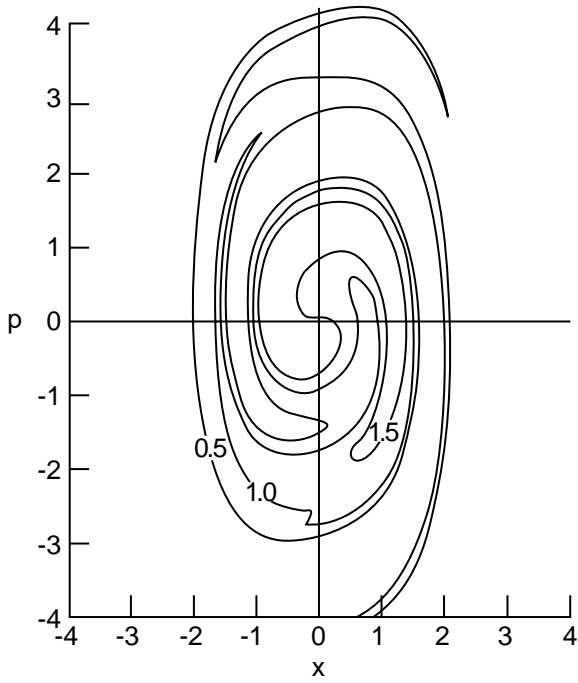


(b) Exact quantum motion.

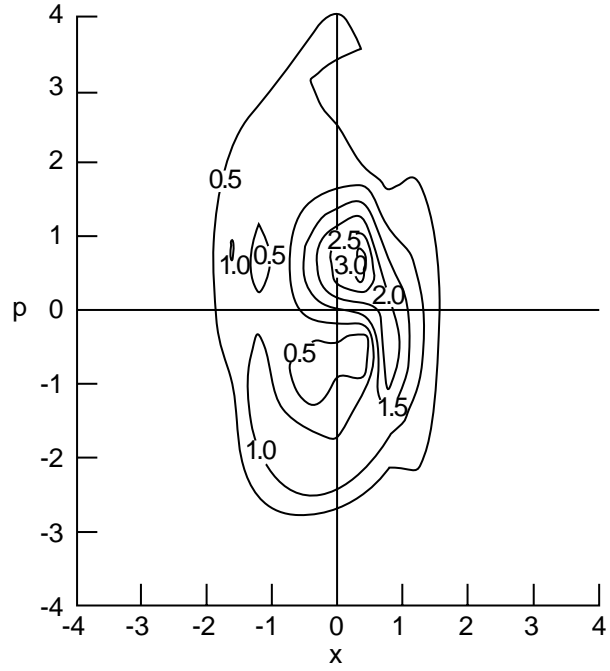


(c) Monte Carlo simulation.

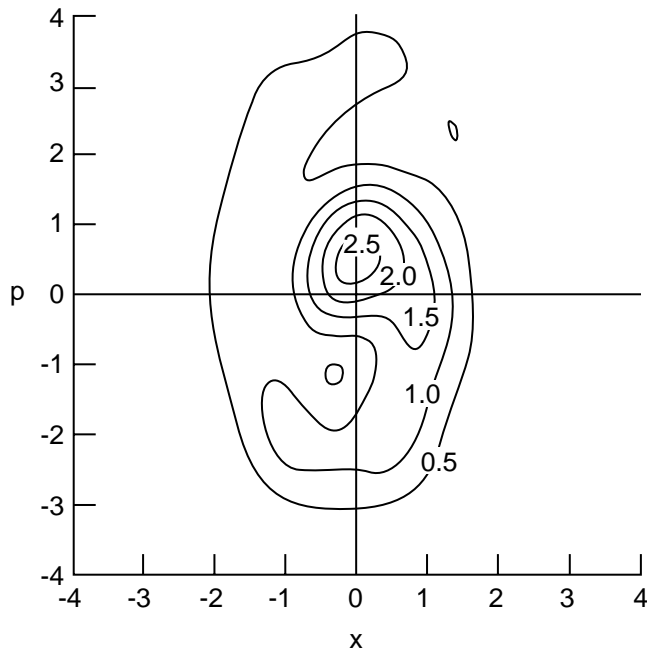
Figure 13. Contour plots of f_ω/β at levels of 0.5, 1.0, and 1.5 for $\beta = 0.5$, $k = 0.5$, Grid size = 0.3, and $\alpha' = 0.3$ at $t = 4\pi$ for a mixed state. The symbols x and p denote the position and momentum coordinates, respectively.



(a) Classical motion.



(b) Exact quantum motion.



(c) Monte Carlo simulation.

Figure 14. Contour plots of f_ω/β at levels of 0.5, 1.0, and 1.5 for $\beta = 0.25$, $k = 0.5$, Grid size = 0.3, and $\alpha' = 0.3$ at $t = 3\pi$ for a mixed state. The symbols x and p denote the position and momentum coordinates, respectively.

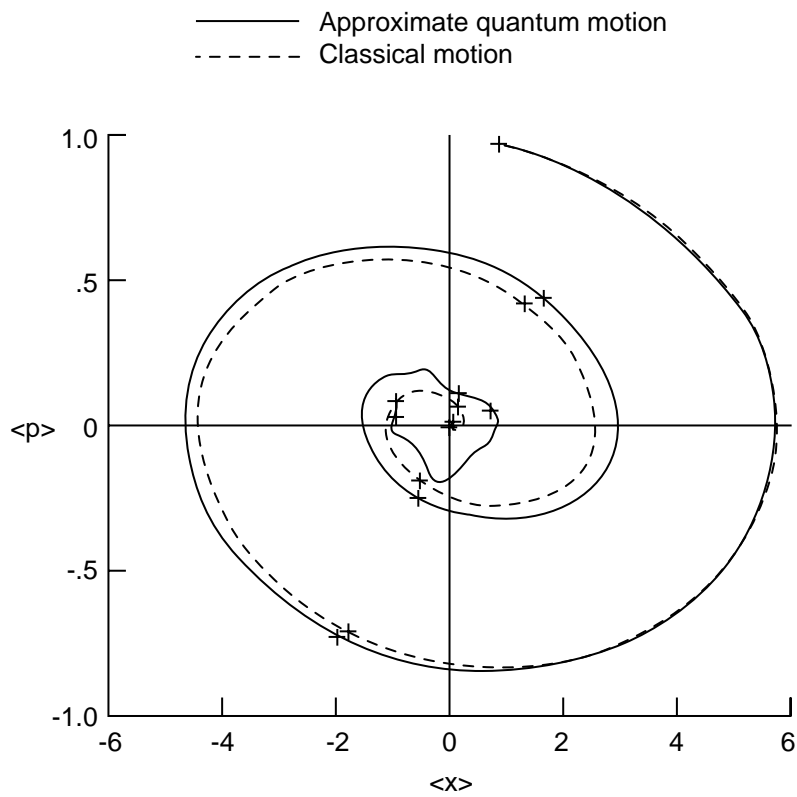


Figure 15. First moments of Wigner distribution function ($\langle x \rangle, \langle p \rangle$) with $k = 0.5$ and $\beta = 0.5$ over a period of time $0-4\pi$. The cross (+) on the curves follows equal intervals of time.

REPORT DOCUMENTATION PAGE			Form Approved OMB No. 0704-0188	
Public reporting burden for this collection of information is estimated to average 1 hour per response, including the time for reviewing instructions, searching existing data sources, gathering and maintaining the data needed, and completing and reviewing the collection of information. Send comments regarding this burden estimate or any other aspect of this collection of information, including suggestions for reducing this burden, to Washington Headquarters Services, Directorate for Information Operations and Reports, 1215 Jefferson Davis Highway, Suite 1204, Arlington, VA 22202-4302, and to the Office of Management and Budget, Paperwork Reduction Project (0704-0188), Washington, DC 20503.				
1. AGENCY USE ONLY (Leave blank)	2. REPORT DATE February 1994	3. REPORT TYPE AND DATES COVERED Technical Paper		
4. TITLE AND SUBTITLE Stochastic Solution to Quantum Dynamics			5. FUNDING NUMBERS WU 199-45-16-11	
6. AUTHOR(S) Sarah John and John W. Wilson				
7. PERFORMING ORGANIZATION NAME(S) AND ADDRESS(ES) NASA Langley Research Center Hampton, VA 23681-0001			8. PERFORMING ORGANIZATION REPORT NUMBER L-17295	
9. SPONSORING/MONITORING AGENCY NAME(S) AND ADDRESS(ES) National Aeronautics and Space Administration Washington, DC 20546-0001			10. SPONSORING/MONITORING AGENCY REPORT NUMBER NASA TP-3408	
11. SUPPLEMENTARY NOTES John: ViGYAN, Inc., Hampton, VA; Wilson: Langley Research Center, Hampton, VA.				
12a. DISTRIBUTION/AVAILABILITY STATEMENT Unclassified-Unlimited Subject Category 93			12b. DISTRIBUTION CODE	
13. ABSTRACT (Maximum 200 words) The quantum Liouville equation in the Wigner representation is solved numerically by using Monte Carlo methods. For incremental time steps, the propagation is implemented as a classical evolution in phase space modified by a quantum correction. The correction, which is a momentum jump function, is simulated in the quasi-classical approximation via a stochastic process. In this paper the technique, which is developed and validated in two- and three-dimensional momentum space, extends an earlier one-dimensional work. Also, by developing a new algorithm, the application to bound state motion in an anharmonic quartic potential shows better agreement with exact solutions in two-dimensional phase space.				
14. SUBJECT TERMS Quantum dynamics; Monte Carlo methods			15. NUMBER OF PAGES 37	
			16. PRICE CODE A03	
17. SECURITY CLASSIFICATION OF REPORT Unclassified	18. SECURITY CLASSIFICATION OF THIS PAGE Unclassified	19. SECURITY CLASSIFICATION OF ABSTRACT	20. LIMITATION OF ABSTRACT	